

Project information	
Project full title	EuroSea: Improving and Integrating European Ocean Observing and Forecasting Systems for Sustainable use of the Oceans
Project acronym	EuroSea
Grant agreement number	862626
Project start date and duration	1 November 2019, 50 months
Project website	<a href="https://www.eurosea.eu">https://www.eurosea.eu</a>

Deliverable information	
Deliverable number	D7.3
Deliverable title	<b>Estimate of magnitude and drivers of regional carbon variability for both regions</b>
Description	Identification of key drivers for the observed changes in carbon uptake at the convection sites
Work Package number	WP7
Work Package title	Ocean Climate Indicators Demonstrator
Lead beneficiary	CNRS
Lead authors	Pierre Testor, Thibaut Wagener, Anthony Bosse, Remy Asselot, Virginie Thierry, Johannes Karstensen
Contributors	Soeren Thomsen, Lidia Carracedo, Karina von Schuckmann, Maciej Telszewski
Due date	31.10.2022
Submission date	21.12.2022
Comments	Due to Covid and travel restrictions, this work required much more preparatory and asynchronous work than initially anticipated. In addition, the work and preparation of the document was complicated by staff changes, which ultimately led to a delayed submission.



This project has received funding from the European Union's Horizon 2020 research and innovation programme under grant agreement No. 862626.

## Table of Contents

Executive summary.....	1
1. The need for knowledge on ocean carbon uptake and storage and its variability .....	2
2. Observational and methodological approaches.....	6
2.1. Estimating DIC and $C_{\text{ant}}$ from Temperature, Salinity and Oxygen profiles .....	6
2.2. Estimating carbon content variability using a model/data synthesis approach .....	8
2.3. Estimating variability of dissolved gas in boundary current systems.....	9
3. Seasonal, interannual and spatial carbon variability.....	10
3.1. Seasonal variability .....	10
Total inorganic carbon pool.....	10
Anthropogenic carbon .....	13
Dissolved gases in the Deep Western Boundary Current.....	13
3.2. Interannual variability .....	14
Total inorganic carbon pool.....	14
Anthropogenic carbon .....	17
Dissolved gases in the Deep Western Boundary Current.....	19
3.3. Spatial variability .....	20
3.4. Quantitative aspects through modelling.....	24
4. Conclusion and global implications .....	28
References.....	30

## Executive summary

This deliverable provides an overview of EuroSea outcomes related to interior ocean carbon variability in deep convection areas in order to assess the linkage of these processes for the use in national climate action (NCA) plans delivered in the framework of the Paris Agreement. In summary, large-scale connectivity in the ocean does not allow clear delineation of patterns of regional carbon uptake across national boundaries, limiting an assessment of the Exclusive Economic Zones (EEZ) in light of NCA plans. This problem becomes already clear by a simple scale estimation: considering sluggish, open ocean (away from continental boundaries) advection speeds of 2 cm/s result in a “relocation” of any water parcel by roughly 630 km per year (or 3150 km in 5 years Paris Agreement carbon auditing period) and crossing national borders easily.

Knowing changes in the global ocean carbon uptake is of great importance for the preparation of NCA plans. This is because the NCA plans are motivated by the globally averaged atmospheric CO<sub>2</sub> concentration, which is the sum of all sources and sinks and including the ocean sink. In case of decrease in the oceanic sink (e.g., IPCC, 2021), more CO<sub>2</sub> will remain in the atmosphere and consequently nations will need to formulate their NCA plans with increased ambition in order to meet the CO<sub>2</sub> target defined in the Paris Agreement. In this deliverable key approaches for the assessment of the global ocean carbon uptake have been applied to ocean areas. The observational requirements for applying statistical approaches (i.e., artificial neural networks, Fourier et al., 2020) to reconstruct dissolved inorganic carbon (DIC) from oxygen, nutrient and hydrographic data are analysed. It is shown that even small changes in the DIC content determined in this way can be linked to anthropogenic increases in atmospheric carbon (C<sub>ant</sub>). Furthermore, it has been shown that multilinear regression techniques can be used to produce maps of ocean surface carbon fluxes at very high spatial resolution, which in turn can provide a much more accurate estimate of regional CO<sub>2</sub> uptake (or release). Finally, a quantification of the redistribution of dissolved gases in boundary current systems could be investigated by following recommendations for observational methods stemming from this deliverable.

This deliverable recommends improvement of carbon sampling in all nations EEZ regions and following global standards. Because the objective targets a global assessment, the data must be disseminated rapidly and in a FAIR fashion to enable further global integration (e.g., global carbon budget). A need for defining responsibilities for such global integration and the resourcing is required. It is recommended to make use of statistical methods to create surface and interior carbon parameter distributions via multiparameter approaches with a sufficient amount of reference data (e.g., co-located DIC, oxygen, nutrients, chlorophyll-a, hydrography). In the light of the ongoing crisis related to global availability of the Certified Reference Materials (CRMs) for carbonate system measurements, provision of European-produced material becomes critical to enable traceability of future measurements. Nations should be encouraged to provide appropriate resources by means of corresponding European directives. Example for such national commitments is the collection of reference data in the framework of the Common Fisheries Policy<sup>1</sup>.

---

<sup>1</sup> [https://oceans-and-fisheries.ec.europa.eu/policy/common-fisheries-policy-cfp\\_en](https://oceans-and-fisheries.ec.europa.eu/policy/common-fisheries-policy-cfp_en)

## 1. The need for knowledge on ocean carbon uptake and storage and its variability

Since the industrial revolution, human activities have emitted large amounts of carbon dioxide (CO<sub>2</sub>) into the atmosphere, distinct as “anthropogenic carbon” (C<sub>ant</sub>). Via air-sea gas exchange, the ocean has taken up a quarter of these C<sub>ant</sub> emissions (Friedlingstein et al., 2022), becoming the only true net sink for C<sub>ant</sub> (Sabine et al., 2004). The ocean is therefore an important regulator for global warming. The Paris Agreement has set a global temperature target to limit the global temperature increase below 2°C of warming by the end of this century. All signatory countries of the Paris Agreement agreed to commit national actions that sufficiently limit C<sub>ant</sub> emissions to a level that will attain the global temperature target (Figure 1). The approach is based on the observation that global warming increases almost linearly with the total amount of C<sub>ant</sub> emissions since the beginning of the industrial revolution.

The efficiency of the ocean to uptake carbon has a major impact on global, European and national CO<sub>2</sub> budgets (Figure 1). In turn, multiannual carbon variability in Exclusive Economic Zones (EEZ) may eventually also be considered in national climate action plans of countries in the framework of the Paris Agreement (Karstensen et al. 2021). It is of value to understand the potential drivers for multiannual carbon variability and the observational needs that are related to a quantification of the variability. The work in EuroSea 7.1. focuses on the assessment of ocean observing needed for estimating carbon variability in two deep water formation areas: the subpolar North Atlantic gyre and the North Western Mediterranean Sea.

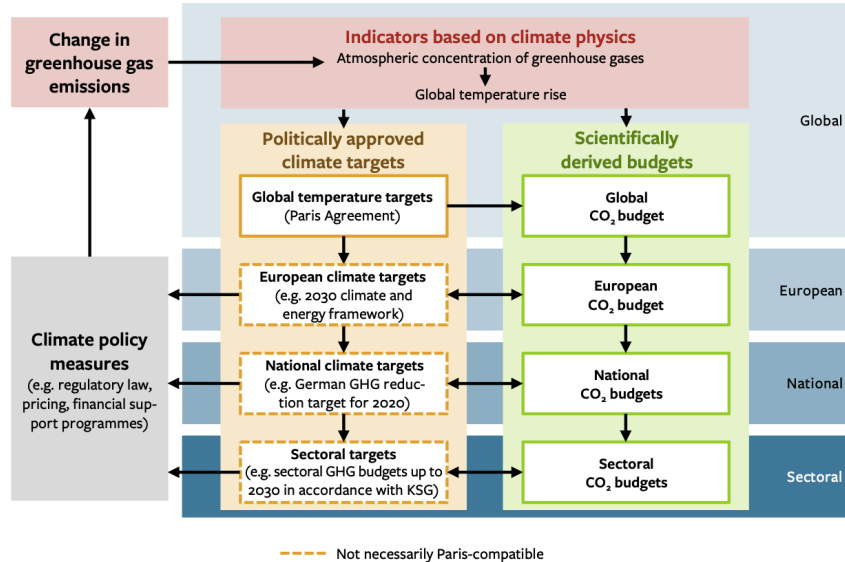


Figure 1. The CO<sub>2</sub> budget as the basis for existing climate targets on different levels (here done for the example of Germany). KSG: Federal Climate Change Act. From: The German Advisory Council on the Environment (SRU) Environmental Report 2020, Chapter 2: Using the CO<sub>2</sub> budget to meet the Paris climate targets.

In general, the biological carbon pump creates a low-to-high gradient of dissolved inorganic carbon (DIC) profile in the ocean. However, the physical pump that is tightly linked to ocean dynamics will alter this picture substantially. In deep convection regions, the DIC distribution can be completely disrupted by the complex ocean dynamics and uptake patterns. Likewise, the lateral transport of DIC influences the local vertical DIC profile. The total DIC pool is the sum of the natural (C<sub>natural</sub>) and anthropogenic carbon components. Although the latter represents about 0.5% of the total DIC pool (Davila et al., 2022), the uptake of C<sub>ant</sub> highly

influences the aquatic environment by changing the chemical properties of the ocean (Doney et al., 2020). It also is of interest for carbon studies to consider oxygen observations (Vachon et al. 2020). Oxygen is biologically linked to carbon, for instance during photosynthesis which simultaneously uses carbon and generates oxygen or during remineralization of organic matter in the ocean interior when oxygen is respired and DIC enriched. Because oxygen observations can be done with great accuracy and stability using autonomous sensors (Bittig et al, 2018a), the global ocean oxygen database has significantly grown over the past decade and is now very large. Given a covariability in oxygen and DIC, oxygen can provide a very good proxy for local and regional carbon variability (Bittig et al, 2018b), but of course not necessarily for the  $C_{ant}$  part of the DIC.

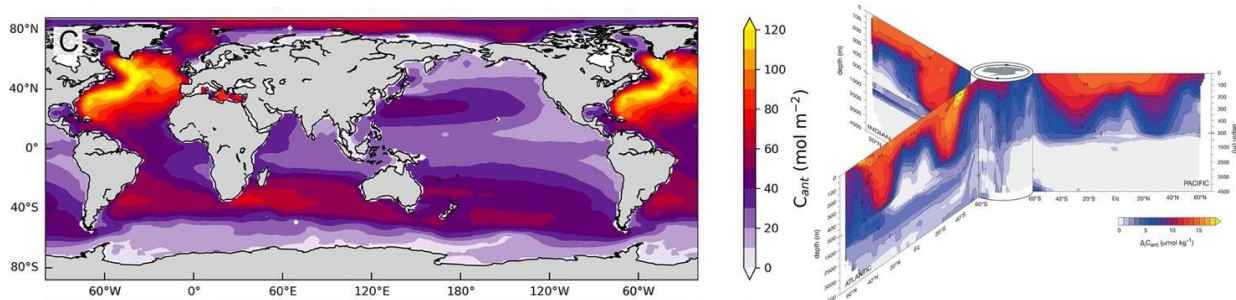


Figure 2. Left panel: Anthropogenic carbon ( $C_{ant}$ ) column inventory produced by the OCIM control “inversion” for 2010. Source: Davila et al. (2022). Right panel: Vertical sections of the change (1994–2007) in anthropogenic carbon,  $\Delta t C_{ant}$ , centred at the Southern Ocean. Source: Gruber et al. (2019).

Deep convection regions, such as the Labrador Sea located at high latitudes in the Atlantic Ocean, are considered large sinks for atmospheric  $\text{CO}_2$  due to strong cooling and high primary production leading to long, or even persistent, periods of deficit compared to the atmosphere (Takahashi et al., 2002). In these regions, large amounts of atmospheric  $\text{CO}_2$  captured at the surface and biologically fixed carbon are transferred to the deep ocean during intense vertical mixing periods (DeGranpre et al., 2006; Körtzinger et al., 2008). On the other hand, respired organic carbon remaining above the winter mixing depth can be ventilated back to the surface during the following winter (DeGranpre et al., 2006; Körtzinger et al., 2008; Palevsky and Nicholson, 2018). Lateral transport, often associated with the restratification of the water column, the dispersion of the newly formed dense water and/or the exchanges with boundary currents, also greatly contributes to the budget of water masses and their biogeochemical contents (Wolf et al., 2018; Koelling et al., 2022).

The northwestern region of the semi-enclosed Mediterranean Sea is located at mid-latitudes and connected to the Atlantic Ocean through the narrow Gibraltar Strait. It is one of the regions where deep convection occurs (Mertens and Shott, 1998; Béthoux et al., 2002). In this region, a basin-scale cyclonic gyre is associated with a doming of isopycnals. The surface density increases in winter, due to cold and dry northerly winds, which produces instabilities of the water column leading to convective mixing of surface waters with deeper waters. The interannual variability of the magnitude and spatial extent of the convection process is driven by both the strength of the air-sea heat flux and the preconditioning corresponding to the pre-winter hydrological properties of the water masses (Houpert et al., 2016; Somot et al., 2016; Estournel et al., 2016; Margirier et al., 2020). With regards to the biogeochemical processes, the region is characterised at the sea surface by a first and moderate phytoplankton bloom in fall, interrupted by deep winter mixing, and a secondary abrupt phytoplankton bloom, following deep winter mixing which has supplied inorganic nutrients in the euphotic layer (Lavigne et al., 2013; Ulses et al., 2016; Kessouri et al., 2017). At the annual scale, the

net community production (NCP, defined as the gross primary production minus the community respiration) was found positive leading to an autotrophic status of the area (Ulses et al., 2016; Coppola et al., 2018). The downward export of organic carbon and its interannual variability have been related to the intensity of the deep convection and the bloom (Heimbürger et al., 2013; Herrmann et al., 2013; Ulses et al., 2016).

The distribution of  $C_{\text{ant}}$  is not homogeneous over the global ocean (Figure 2, left panel). The North Atlantic Ocean is one of the major carbon sinks in the global ocean (Goris et al., 2022, Davila et al. 2022) and the most important region for the deep injection and storage of  $C_{\text{ant}}$  is in the Labrador and Irminger Sea (Sabine et al. 2004, Gruber et al., 2019, Davila et al., 2022). This particular region accounts for 23-38% of the total oceanic  $C_{\text{ant}}$  (Sabine et al., 2004, Steinfeldt et al., 2009) and even more importantly is the direct transfer of the  $C_{\text{ant}}$  into dense/deep waters. The North Atlantic Ocean is thus a key player in mediating the ongoing global warming. While the North Western Mediterranean Sea is a more marginal carbon sink than the North Atlantic due to its smaller surface, the Mediterranean water column inventory of  $C_{\text{ant}}$  is considerably higher than other oceanic areas at the same latitude (Lee et al., 2011). This is generally considered to be related to the high temperature and alkalinity content of the water column and the active overturning circulation (Schneider et al. 2010).

The concentration of  $C_{\text{ant}}$  is not homogeneously distributed throughout the water column (Figure 2, right panel). In direct contact with the atmosphere where the air-sea flux occurs, the ocean surface contains the highest  $C_{\text{ant}}$  concentrations but these concentrations decrease with depth. Over time, and mirroring the ongoing increase in atmospheric CO<sub>2</sub>, the water-column  $C_{\text{ant}}$  concentration is increasing (e.g., Figure 2, left panel). This result indicates that deep oceanic regions, where there was initially no anthropogenic signature, start showing significant  $C_{\text{ant}}$  concentrations. Due to deep water mass formation (winter convection) and associated thermohaline circulation (Atlantic Meridional Overturning Circulation, AMOC), this is particularly true for the North Atlantic (Pérez et al., 2018). For instance, in this region,  $C_{\text{ant}}$  concentration has increased by ~70% between 1991 and 2016 at 1500m depth (Figure 3). However, in marginal seas such as the Mediterranean Sea, the entire water column contains  $C_{\text{ant}}$  due to the short residence time of the waters composing this basin. For instance, at the beginning of the 21st century, high  $C_{\text{ant}}$  concentrations of 70  $\mu\text{mol/kg}$  were estimated in the upper water column. Even in the oldest waters of the eastern Mediterranean, the concentration of  $C_{\text{ant}}$  reaches 20  $\mu\text{mol/kg}$  (Schneider et al. 2010). Estimates of  $C_{\text{ant}}$  have also been made with monthly observations accumulated over more than a decade at the DYFAMED time-series station (Touratier and Goyet 2009) to estimate the temporal evolution of  $C_{\text{ant}}$  in the western Mediterranean Sea. This objective was reached by using recognized interpolation procedures to reconstruct the incomplete distributions of measured total dissolved inorganic carbon and total alkalinity. These reconstructed fields, associated with those available for dissolved oxygen and temperature, were used to estimate the distribution of  $C_{\text{ant}}$ . This was done with the TrOCA (Tracer combining Oxygen, inorganic Carbon, and total Alkalinity) approach and the main results indicate that (1) the concentrations of  $C_{\text{ant}}$  are much higher than those found in the Atlantic Ocean (the minimum concentration at the DYFAMED site is 50  $\text{mmol kg}^{-1}$ ), and (2) the temporal trend for anthropogenic CO<sub>2</sub> is decreasing, especially in the intermediate and the deep layers of the water column at the DYFAMED site. This decrease in  $C_{\text{ant}}$  is significantly correlated with a decrease in the dissolved oxygen and with an increase in both salinity and temperature. In the light of different studies that propose explanations for the observed increases in salinity and temperature that occurred in the western basin since the 1950s, they conclude that the decrease in  $C_{\text{ant}}$  probably resulted from an invasion of old water masses. The Eastern Mediterranean Transient (EMT) could have played an important role in the observed decrease in  $C_{\text{ant}}$  concentrations at the DYFAMED site.

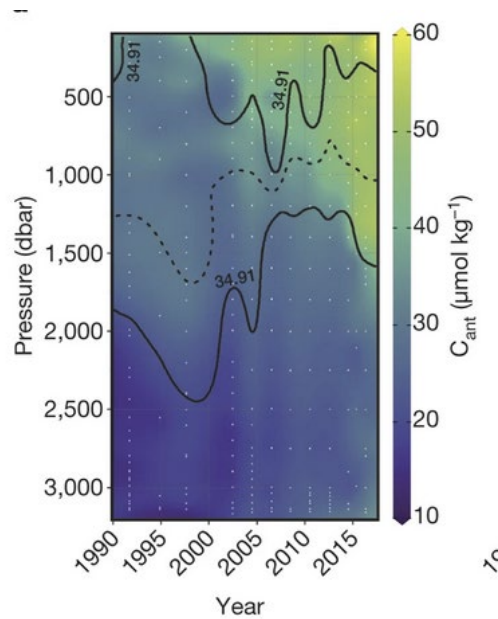


Figure 3. Time evolution from 1991 to 2016 of  $C_{\text{ant}}$  (colour contour); the isohaline 34.91 (continuous black lines) and the salinity minimum (dotted black line) are shown. Source: Pérez et al. (2018).

During decades, studies on the oceanic carbon have been mostly performed through the coordination of oceanographic cruises that collect samples along the water column and perform accurate measurements. High quality databases of carbonate chemistry (e.g., GLODAPv2; Olsen et al., 2019) have been generated and they allow to obtain a “snapshot” of the oceanic carbon content. In addition, continuous shipboard surface  $p\text{CO}_2$  measurements on research and opportunity vessels allow to have annual estimates of air-sea  $\text{CO}_2$  exchanges. These observations are crucial to get a global comprehension of the oceanic carbon content.

To date,  $C_{\text{ant}}$  estimates are based on ship-based measurements. These ship-based methods are gathered into two main groups on the basis of the variables needed to compute  $C_{\text{ant}}$ . The first group considers carbon-based methods (e.g., Sabine et al., 2004, Touratier et al. (2007), Gruber et al., 2019, Pérez et al., 2013) and the second group considers tracer-based method (e.g., Khatiwala et al., 2013, Lauvset et al., 2016, Davila et al., 2022). These methods are used to produce oceanic 3D (lat, lon, depth)  $C_{\text{ant}}$  inventory maps and climatologies but with a sparse spatial and temporal resolution. Since  $C_{\text{ant}}$  concentrations in the ocean cannot be directly measured, it is very difficult to assess the accuracy of the various estimates. Until now, only comparisons among the various approaches and hypotheses have been used to estimate the uncertainties of the results. For example, anthropogenic tracers (here: CFC-11,  $^{14}\text{C}$  and  $^3\text{H}$ ) can be used to assess the relevance of three estimates of  $C_{\text{ant}}$  distributions based upon very different hypotheses.

In respect to the outlined requirement on knowledge about the ocean carbon uptake from a global to a regional (national) scale and in line with the objective of Task 7.1, it becomes apparent that observational means are needed to better estimate the ocean carbon content and its variability. We demonstrate here how the combination of core hydrographic variables (temperature, salinity and oxygen) from ship or novel autonomous platforms (e.g., Argo floats and gliders) at an unprecedented spatial and temporal coverage, with cutting edge statistical analysis (e.g., artificial neural networks (NNs), Fourrier et al. 2020), opens up a new range of resources for the study of the ocean carbon cycle. This new approach permits refining oceanic carbon assessment and studying processes at the seasonal and inter-annual scale that are essential to

understand the overall dynamics of the oceanic carbon cycle. It also opens the possibility for operational oceanic carbon assessment.

As deep convection plays a key role in the circulation and biogeochemical cycles and thus can directly affect the carbon content of large oceanic areas, we additionally show how this approach allows a more detailed vision of the carbon and  $C_{\text{ant}}$  distribution, storage and pathways and their evolution in regions of intense water mass mixing and complex circulation like the subpolar North Atlantic gyre and the western Mediterranean Sea than the ones provided by the existing climatologies.

## 2. Observational and methodological approaches

In general, the ocean absorbs carbon via two mechanisms. First, it takes up carbon via the biological carbon pump, defined as the uptake of  $\text{CO}_2$  in the upper ocean by marine biota and the sinking of this carbon in the abyssal ocean (Turner, 2015). Second, besides marine biota, the ocean also takes up carbon via the physical pump, meaning that carbon is also stored via an increase in the ocean inventory, originating from a balance between uptake and transport processes in the ocean. The interplay between biological and physical pump, ocean circulation and paired with the increasing atmospheric  $\text{CO}_2$  as a boundary condition determine the carbon distribution and its variability in the ocean.

### 2.1. Estimating DIC and $C_{\text{ant}}$ from Temperature, Salinity and Oxygen profiles

To study DIC and  $C_{\text{ant}}$  distribution in the North Atlantic Ocean, we use Argo-O<sub>2</sub> data in combination with NNs and carbon-based back calculation methods. First, we rely on predictive NNs to derive the biogeochemical variables required to calculate  $C_{\text{ant}}$ . We use ESPER\_NN (Carter et al., 2021) to predict the macronutrients ( $\text{PO}_4^{3-}$ ,  $\text{Si}(\text{OH})_4$ ,  $\text{NO}_3^-$ ) from the Argo-O<sub>2</sub> data. We also use CONTENT (Bittig et al., 2018b) to derive dissolved inorganic carbon (DIC) and total alkalinity (At) from the Argo-O<sub>2</sub> data. We rely on CONTENT to estimate the carbon variables because this neural network assures that DIC and At are internally consistent within the carbonate system. Second, to determine  $C_{\text{ant}}$  from the total carbon pool, we use the back-calculation method  $\phi\text{CoT}$  (Pérez et al., 2008). This method is originally developed for deep-water formation regions in the Atlantic Ocean, where the subsurface layer (100-200 m) is chosen as a reference layer for characterising water masses properties at the time of their formation. With this assumption,  $C_{\text{ant}}$  estimates are improved in cold and deep water formation regions subject to strong mixing processes, such as the subpolar North Atlantic gyre. The input variables for this method are the date, location, T, S, O<sub>2</sub> (the Argo variables), the macronutrients (obtained from ESPER\_NN), plus At and DIC (from CONTENT). The errors associated with the input variables propagate through the  $C_{\text{ant}}$  calculations via the Monte Carlo method (Metropolis & Ulam, 1949). The overall uncertainty of our method is  $\pm 5.5 \mu\text{mol/kg}$ .

As a validation of our methodology, we compared the vertical structure and values of DIC concentration in the Irminger Sea estimated from Argo float data between 2010 and 2022 with those estimated from the GLODAPv2.2021 data set (Lauvset et al. 2021) (Figure 4). We also compared Argo-based  $C_{\text{ant}}$  estimates with ship-based measurements acquired during the 2014 GEOVIDE cruise (Asselot et al., in preparation). The overall good agreement between the various estimates gives confidence in our Argo-based DIC and  $C_{\text{ant}}$  estimates.

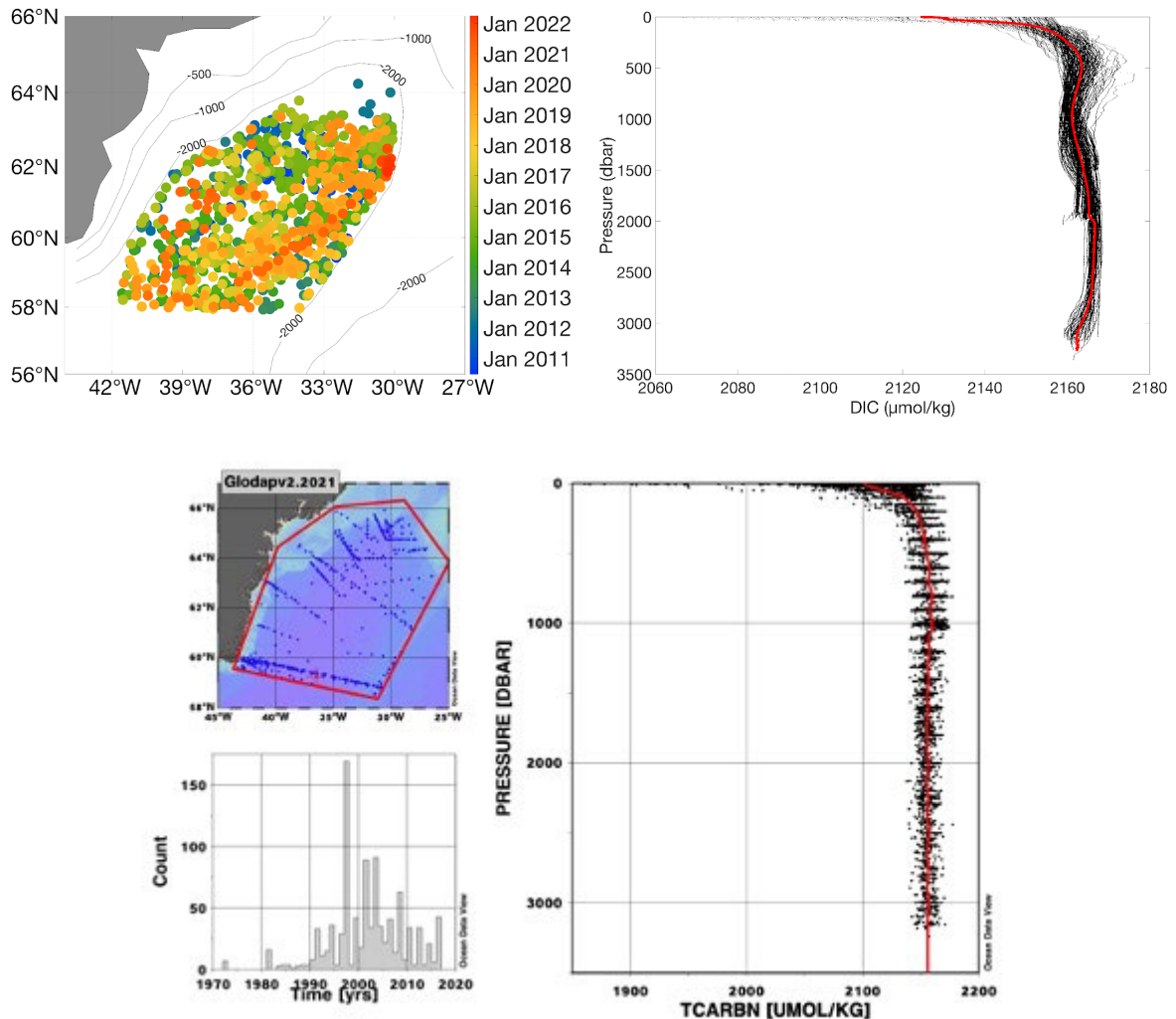


Figure 4. Top left panel: Location of the 1078 Argo-O<sub>2</sub> profiles of our database. The color coding represents the date. Top right panel: Vertical distribution of dissolved inorganic carbon ( $\mu\text{mol/kg}$ ) from Argo data. The black points represent the monthly gridded profiles while the red line represents the mean DIC profile over the study period. Bottom left (upper) panel: GLODAP data grid location in the Irminger Sea (Source data: GLODAPv2.2021, Lauvset et al. 2021). Bottom left (lower) panel: Frequency histogram showing the GLODAP data time coverage. Bottom right panel: Vertical distribution of GLODAP dissolved inorganic carbon ( $\mu\text{mol/kg}$ ) in the Irminger Sea. The black points show the raw data while the red line represents the vertical moving average (ODV statistics).

For the Mediterranean Sea a slightly different method was applied to increase the spatio-temporal coverage of the carbon dataset, CANYON-MED, which is a regional neural network-based method developed to estimate Nutrients and carbonate variables specifically for the Mediterranean Sea. The implementation and validation of this neural network-based method is described in Fourier et al., 2020. It has been trained with the CARIMED (CARbon in the MEDiterranean Sea) data synthesis initiative (Sanleón-Bartolomé et al., 2017) and additional cruises in the whole Mediterranean Sea as well as MOOSE-DYFAMED monthly cruises<sup>2</sup>, while MOOSE-ANTARES<sup>3</sup> was used as an independent data set to validate the approach. CANYON-MED was used to derive carbonate chemistry parameters from the adjusted and validated temperature, salinity and

<sup>2</sup> <https://doi.org/10.17882/43749>

<sup>3</sup> <https://doi.org/10.18142/233>

dissolved oxygen profiles from O<sub>2</sub>-equipped Argo floats and gliders. CANYON-MED has been used at the scale of the entire fleet of floats available in North-Western Mediterranean (Figure 5) to derive carbonate system variables in the Gulf of Lion and the Ligurian Sea to estimate trends over the 2012–2020 period in carbonate chemistry (Fourrier et al. 2022). We also applied the CANYON-MED neural networks on profiles carried out from ships from the MOOSE-GE cruises<sup>4</sup> between 2010 and 2021 and DEWEX in 2013<sup>5</sup>. The use of CANYON-MED on MOOSE-GE and DEWEX data allows to expand the spatial coverage of the carbonate chemistry dataset to the entire deep sea convection area.

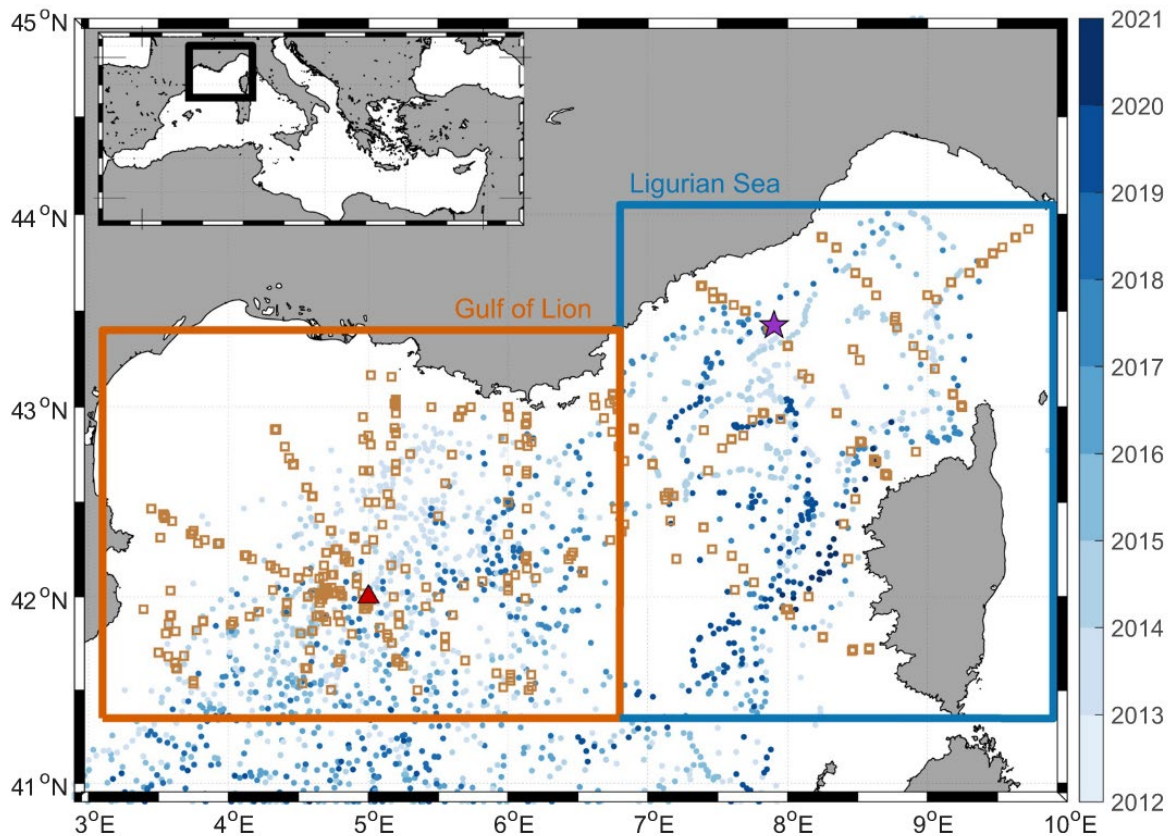


Figure 5. Position of Argo profiling floats profiles equipped with O<sub>2</sub> sensors according to the time of the profile (blue circles), stations from cruises (brown squares), and of the LION (red triangle) and DYFAMED (purple star) mooring sites in the Gulf of Lion (orange box) and Ligurian Sea (blue box), respectively (From Fourrier et al. 2022).

## 2.2. Estimating carbon content variability using a model/data synthesis approach

The seasonal cycle and annual budget of DIC in the deep convection area of the North Western Mediterranean Sea is investigated through a 3-dimensional coupled physical-biogeochemical model. Ulses et al. (in review) used the biogeochemical model Eco3M-S forced offline by daily outputs of the 3D hydrodynamic model SYMPHONIE (Marsaleix et al., 2008). The carbonate chemistry model developed by Soetaert et al. (2007) was added to study the carbonate chemistry. The internal variation, air-sea flux, biological term, lateral physical term, the vertical advection and mixing of DIC were calculated by the model.

<sup>4</sup> <https://doi.org/10.18142/235>

<sup>5</sup> <https://doi.org/10.17600/13020010>

The chosen period for the simulation is September 2012 to September 2013 because of the particularly high availability of carbon data during this period. High frequency data collected from the BOUSSOLE mooring site<sup>6</sup> and monthly vertical profiles from the MOOSE-DYFAMED site were used to evaluate the time evolution of the model. The horizontal and vertical distribution of the simulated DIC concentration were compared with in situ observations collected during three cruises following the same MOOSE-GE sampling grid that were carried out in the framework of the DEWEX project to study the deep convection and bloom processes over an annual cycle (preconditioning, mixing and spreading phases). The performance of the coupled model is evaluated in Ulses et al. (in review) and is considered as satisfactory.

### 2.3. Estimating variability of dissolved gas in boundary current systems

For the transport and export of dissolved gas in the Western Boundary Current system of the Atlantic, which connects directly with the AMOC, oxygen sensors have been added to boundary current arrays (Figure 6). The installations have been pioneered by the partnership between the EuroSea task 7.1 partners GEOMAR and Dalhousie University adding in 2016 oxygen optodes to the 53°N Observatory. This way the dissolved gas transport in the Labrador Sea Water (LSW) and the Northeast Atlantic Deep Water (NEADW) layer could be monitored (Koelling et al. 2022). In 2020 additional oxygen sensors and also pCO<sub>2</sub> sensors were added to a number of moorings in the subpolar gyre that run under the “Overturning in the Subpolar Gyre Program” (OSNAP) umbrella via the project “GOHSNAP” (Figure 6). The data from the sensors is used to study seasonal variability of dissolved oxygen in the boundary current. Furthermore, a coherence analysis is used to quantify the energy content and phase shift between hydrography parameters (temperature and salinity) and oxygen.

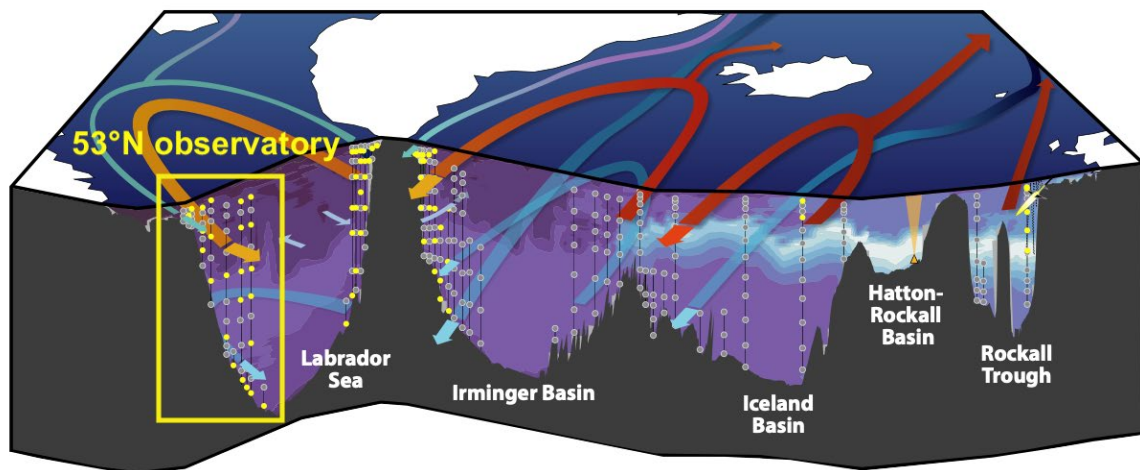


Figure 6. Schematic of the circulation in the subpolar North Atlantic (colored arrows). Locations of OSNAP moorings are shown (black lines) with temperature, salinity, currents at various depths (gray circles). Added GOHSNAP and partner oxygen sensors are in yellow. The shading on the section represents oxygen concentration (after Atamanchuk et al. 2021).

<sup>6</sup> <https://doi.org/10.17882/56709>

### 3. Seasonal, interannual and spatial carbon variability

The work done in EuroSea Task 7.1 resulting in this deliverable addresses the DIC and the small fraction of DIC that accounts for the anthropogenic carbon ( $C_{ant}$ ). In order to bring the different regions together, the results are presented in reference to the time scales of variability - seasonal, inter-annual and trends.

#### 3.1. Seasonal variability

##### Total inorganic carbon pool

Before focusing on the seasonal signal, we consider the vertical structure of the Argo-based monthly-mean DIC values in the Irminger Sea averaged over 2010-2022. The lowest concentration of DIC is found at the surface where it reaches on average a value of  $2120 \mu\text{mol/kg}$  over the whole study period (Figure 7). These low concentrations are due to biological consumption of DIC. Further down, DIC increases at depth via organic matter remineralization. From 300 to 2000 dbar, the 2010-2022 mean DIC concentration is in the range of  $2160$ - $2165 \mu\text{mol/kg}$ . Below, between 2000 and 3000 dbar, the mean DIC concentration is constant, with an averaged value of  $2165 \mu\text{mol/kg}$ .

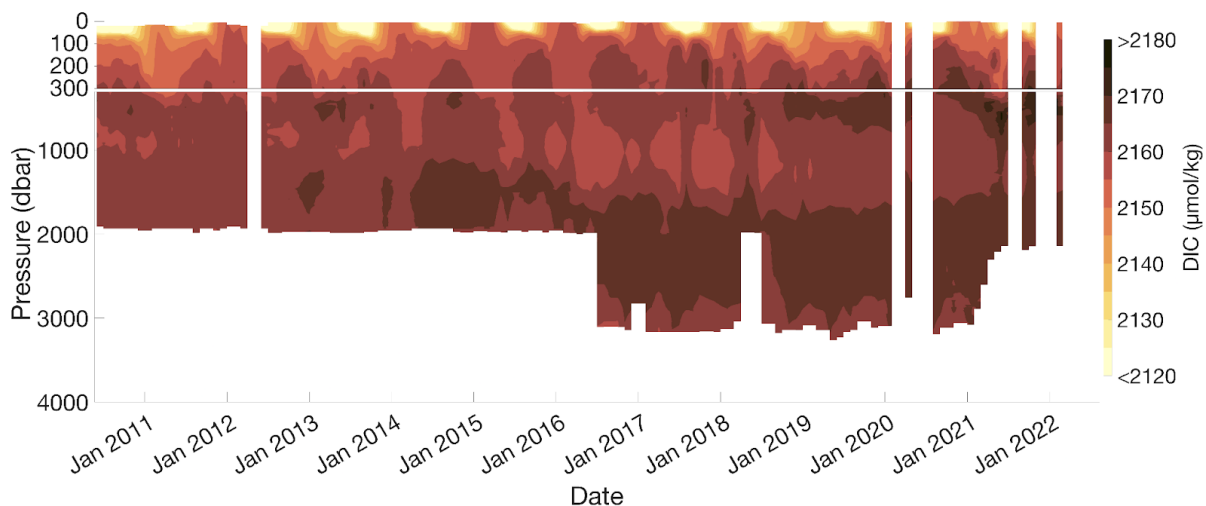


Figure 7. Argo-based dissolved inorganic carbon DIC ( $\mu\text{mol/kg}$ ) in the Irminger Sea from June 2010 to August 2022. The float data displayed on Fig. 4 have been averaged to obtain one DIC profile per month.

The upper Irminger Sea is characterized by a pronounced DIC intra-annual signal (upper 300 dbar, Figure 7). The largest DIC seasonal amplitude ( $\sim 50 \mu\text{mol/kg}$ ) is mostly confined within the first 50 dbar of the water column, representing the euphotic zone (Figure 7, Figure 8). During the winter months, the surface DIC concentration reaches a maximum mean value of  $\sim 2150 \mu\text{mol/kg}$  that progressively decreases throughout the spring and summer months, reaching an averaged minimum value of  $\sim 2100 \mu\text{mol/kg}$  in August (blue line on Figure 8). The amplitude of the seasonal pattern, as well as the mean DIC values, are in good agreement with previous DIC concentrations estimated via ship-based measurements (e.g., Racape et al., 2018; Leseurre et al., 2020). The mechanisms leading to this seasonal pattern are a combination (or interplay) of both physical (seasonal variation in sunlight, sea surface temperature, and mixed layer depth) and biological (spring-summer phytoplankton bloom) processes, which are characteristic from high-latitude oceans (Williams & Follows, 2011). Strong winter mixing and air-sea heat loss enhance the surface DIC concentrations in winter via DIC entrainment from deeper thermocline waters and increased solubility, respectively. As the sunlight and thermic forcings increase from spring to summer, the environmental

conditions (i.e., light availability and stratification) favour an intense phytoplankton bloom (Holliday et al., 2006; Williams & Follows, 2011). As a consequence, DIC is consumed by marine biota via photosynthesis, which, in concurrence with the temperature-driven reduced solubility of the surface waters, leads to a minimum DIC mean concentration in August. Underneath the euphotic zone, the DIC seasonal cycle quickly becomes mostly unnoticeable, with DIC concentration slightly varying through the year (Figure 8).

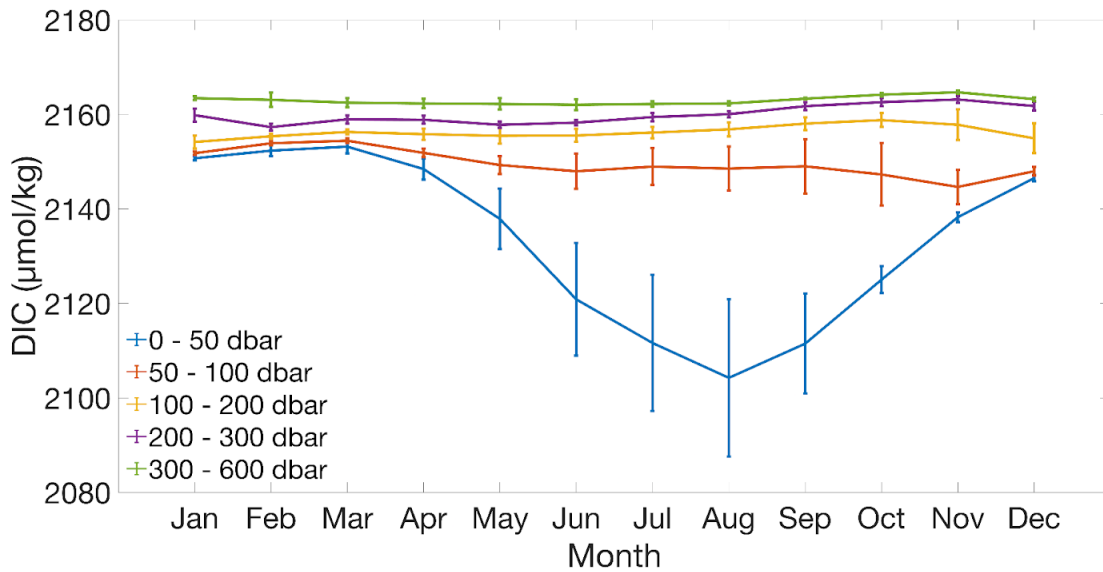


Figure 8. Mean seasonal cycle of Argo-based DIC ( $\mu\text{mol}/\text{kg}$ ) in the Irminger Sea averaged in 5 pressure layers. The data represent the monthly averages over the period June 2010 - August 2022. The error bars account for the standard deviation.

Similar amplitudes of variations are observed in the Mediterranean Sea, where the seasonal cycle is also controlled by the timing of stratification and biogeochemical processes. A seasonal signal can be observed over the entire water column during years of deep-water convection. During the stratified period, surface DIC concentrations are reaching the lowest values ( $2250 \mu\text{mol}/\text{kg}$ ) at the end of the summer period and remain low during autumn. During winter, mixing with intermediate and deep waters increases the surface concentration of DIC up to  $2300 \mu\text{mol}/\text{kg}$  (Figure 9).

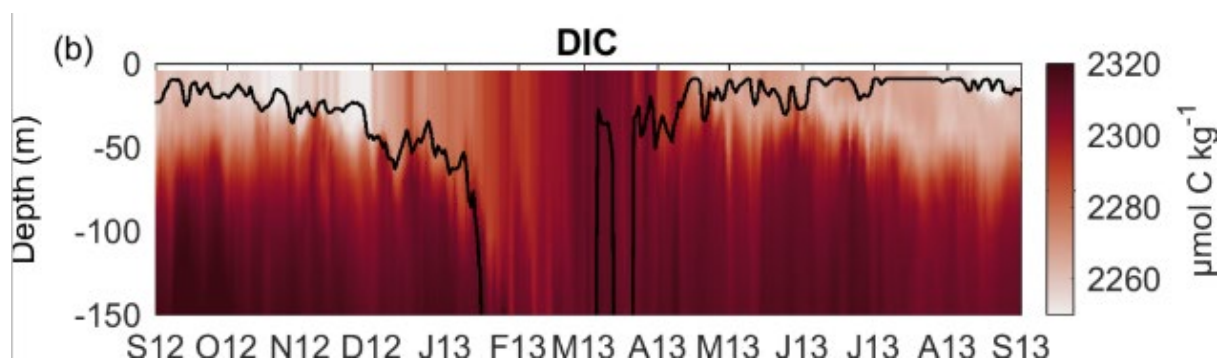


Figure 9. Seasonal variability of dissolved inorganic carbon ( $\mu\text{mol}/\text{kg}$ ) from September 2012 to September 2013 in the north Western Mediterranean deep convection area. The DIC concentration corresponds to the horizontally averaged over the area and the mixed-layer depth (m) is indicated by the black line (From Ulises et al., in rev.).

Figure 10 shows the time evolution of atmospheric and hydrodynamic conditions as well as of surface  $\text{pCO}_2$  and DIC in the deep convection area, while Figure 11 shows budgets according to the different seasons. Based

on the coupled model results, estimates of the driver of the DIC changes can be inferred for the surface waters of the deep convection area. During winter, air sea fluxes and physical transport from the deep ocean are counterbalancing the biological DIC consumption conducting to a DIC enrichment in the surface waters, whereas during Spring the biological consumption is the major sink for surface DIC. During Summer and Fall, the DIC Changes are less pronounced with a small loss of DIC in summer mostly driven by biological uptake through photosynthesis and small gain in fall mostly driven by the excess of respiration over photosynthesis.

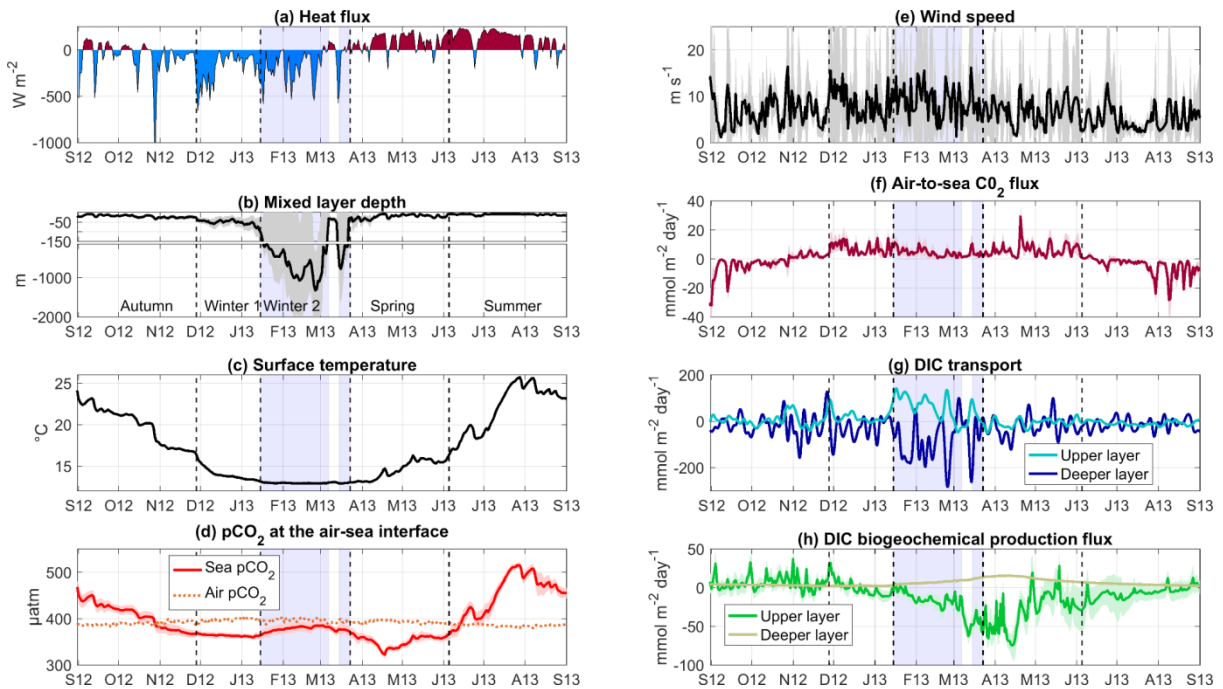


Figure 10. Time series of modelled (a) total surface heat fluxes ( $W m^{-2}$ ), (b) mixed-layer depth (m), (c) sea surface temperature ( $^{\circ}C$ ), (d) sea surface and atmospheric  $pCO_2$  ( $\mu atm$ ), (e) wind speed ( $m s^{-1}$ ), (f) air-to-sea  $CO_2$  flux ( $mmol C m^{-2} day^{-1}$ ), (g) DIC total transport in the upper (light blue) and deeper layer (dark blue) towards the convection area ( $mmol C m^{-2} day^{-1}$ ), and (h) DIC biogeochemical production ( $mmol C m^{-2} day^{-1}$ ) in the upper (green) and deeper (brown) layer. All the parameters are spatially averaged over the convection area (spatial mean in solid line and shaded area for SD). Sources: ECMWF for heat flux and wind speed, SYMPHONIE/Eco3M-S for the other parameters and fluxes. The blue shaded area corresponds to the deep-convection period (period when spatially averaged mixed layer depth  $> 100 m$ ). Note that the range of the y axis varies for the different carbon fluxes, and due to higher values (From Ulses et al., in rev.).

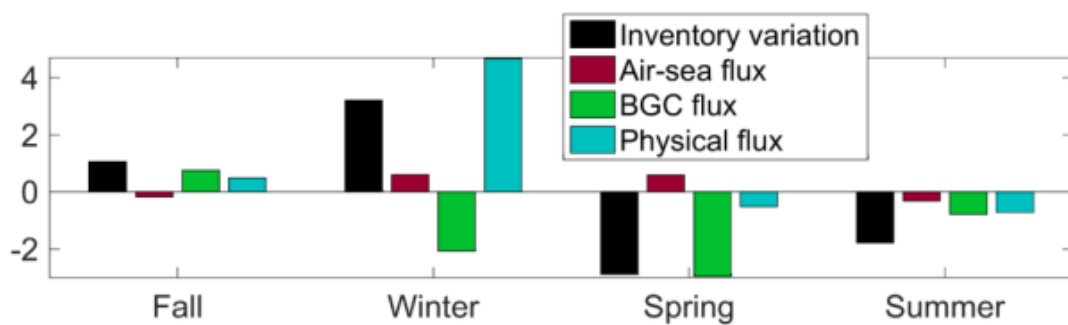


Figure 11. Dissolved inorganic carbon (DIC) inventory in the upper (surface to 150 m) base on seasonal cumulative fluxes and internal variation in (b). Unit:  $mol C m^{-2}$ . (From Ulses et al., in rev.).

## Anthropogenic carbon

Anthropogenic carbon does not exhibit a significant seasonal signal, within the Irminger Sea. Its monthly mean concentration is nearly constant year-round at each depth level (not shown). This highlights that most of the DIC seasonal signal can be attributed to the natural component.

## Dissolved gases in the Deep Western Boundary Current

Given the similarities in oxygen and carbon uptake it is of use to also consider oxygen variability as a proxy for carbon (as outlined above for the  $C_{ant}$  estimate). However, without a focus on the  $C_{ant}$  signal it is informative to consider the full DIC variability if it operates on multiannual time scales, in order to assess the link between oxygen and circulation elements that contribute to the Atlantic Meridional overturning circulation (AMOC), namely the deep western boundary current that encircles the subpolar North Atlantic and is an important export pathway of dissolved gas towards the equatorial Atlantic and further south.

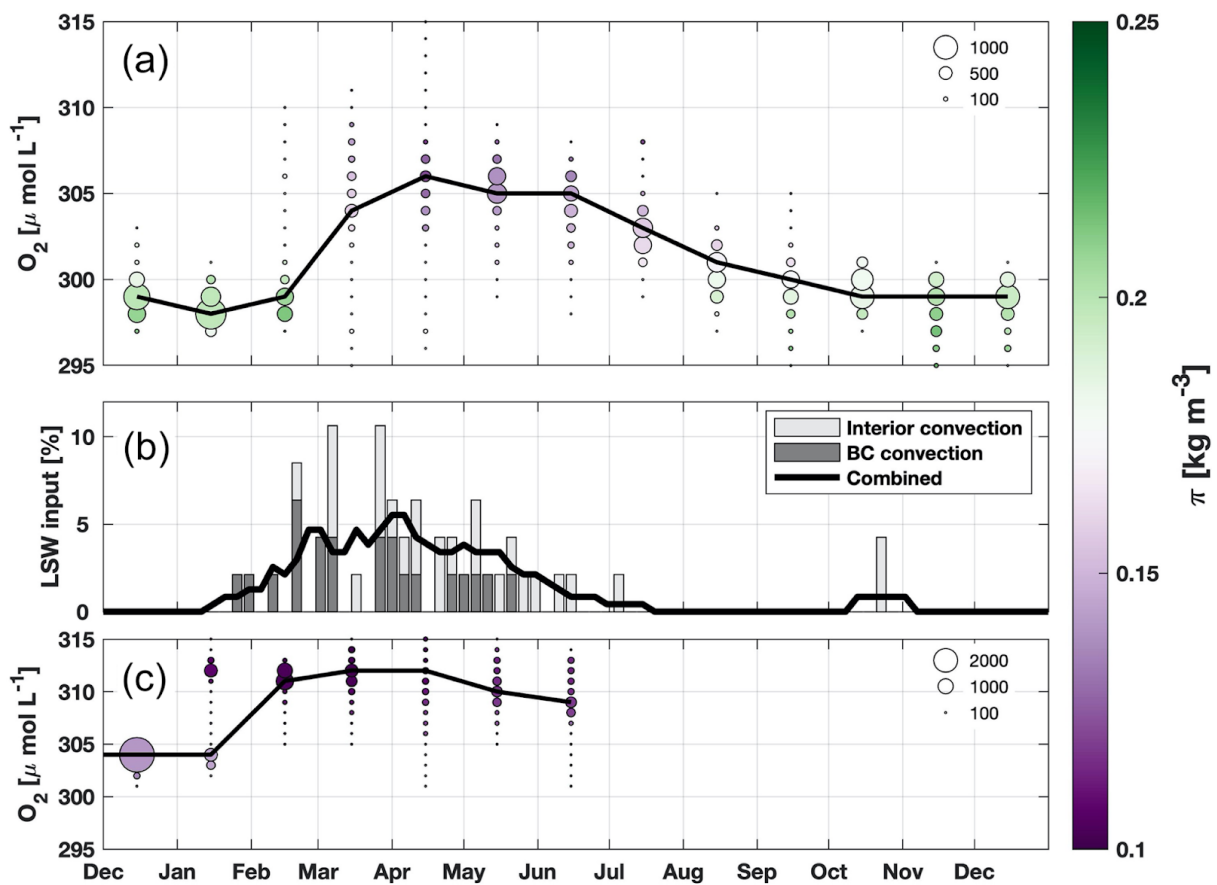


Figure 12. Monthly histogram of oxygen from December 2016 to December 2017 at 610 m depth at the central mooring in the 53°N observatory. The size of each circle corresponds to the number of observations, the black line shows the bin with the highest number of observations for each month, and colors show the mean spiciness of each  $O_2$  bin. (b) Climatological seasonal cycle of LSW input into the boundary current from float data in 5 d bins as a fraction of the total input of LSW over the year. Gray bars show separately the input from boundary and interior convection in each 5 d bin, and the black line shows the combined input smoothed with a five-point running mean. (c) Monthly histogram of oxygen from December 2016 to July 2017 at 500 m depth for the SeaCycler mooring in the deep convection area in the interior of the basin. The size of each circle corresponds to the number of observations, the black line shows the bin with the highest number of observations for each month, and colors show the mean spiciness of each  $O_2$  bin (from Koelling et al. 2022).

The seasonal cycles of oxygen concentration, temperature, and salinity from a 2-year (2016-2018) time series collected by sensors moored at 600m nominal depth in the outflowing boundary current through the 53°N observatory (Figure 6) show a cooling, freshening, and increase in oxygen content of the water flowing out of the basin between March and August (Figure 12). Analysis of Argo float data suggests that this is preceded by an increased input of LSW into the boundary current about 1 month earlier. This input is the result of newly ventilated LSW entering from the interior, as well as LSW formed directly within the boundary current. Together, these results imply that the southward export of newly formed LSW primarily occurs in the months following the onset of deep convection, from March to August, and that this direct LSW export route controls the seasonal oxygen increase in the outflow at 600 m depth. During the rest of the year, properties of the boundary current measured at the 53°N observatory resemble those of Irminger Water, which enters the basin with the boundary current from the Irminger Sea.

### 3.2. Interannual variability

#### Total inorganic carbon pool

Through the period of study, DIC concentration in the upper Irminger Sea (<300 dbar) varies between 2145 and 2155  $\mu\text{mol}/\text{kg}$  (Figure 7, Figure 13). These fluctuations are not significant due to the large standard deviation for the DIC estimates. For the rest of the water column, the year-to-year variations are less than 5  $\mu\text{mol}/\text{kg}$  with no noticeable pattern.

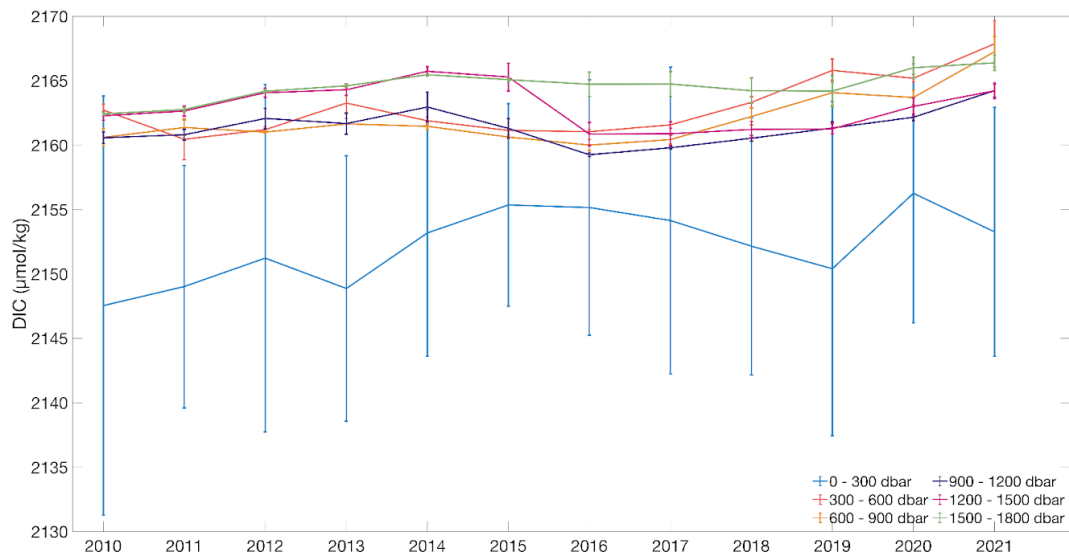


Figure 13. Interannual DIC concentration ( $\mu\text{mol}/\text{kg}$ ) between 2010 and 2021. The water column is divided into 6 layers of 300 dbar.

In the North Western Mediterranean Sea (See Figure 14 & Figure 15 for an example at the LION station), temporal changes in the DIC content of the upper water column are mostly driven by seasonal changes. Under 100 m an increase of DIC over the last ten years is observed with a mean trend of 1.7  $\mu\text{mol.kg}^{-1}.\text{y}^{-1}$ . The increase of DIC at intermediate levels seems to be more pronounced than at the deep level.

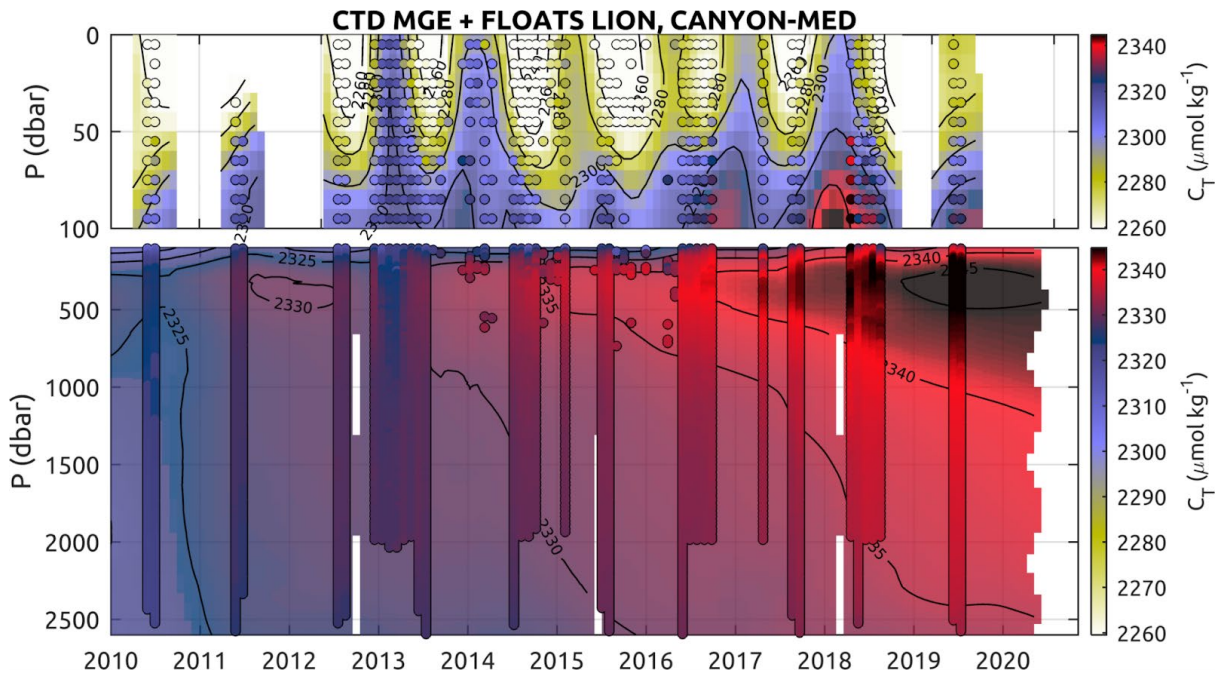


Figure 14. Evolution of the DIC concentration ( $\mu\text{mol}/\text{kg}$ ) between 2010 and 2021 at the LION site ( $42^{\circ}02'N$   $4^{\circ}40'E$ ) in the upper water column (0-100dBar) (Top panel) and in the rest of the water column (100-2500 dBar). DIC concentration are estimated using CANYON-MED applied to the cruise data (MOOSE-GE and DEWEX cruises) and Argo floats in the vicinity of the LION site.

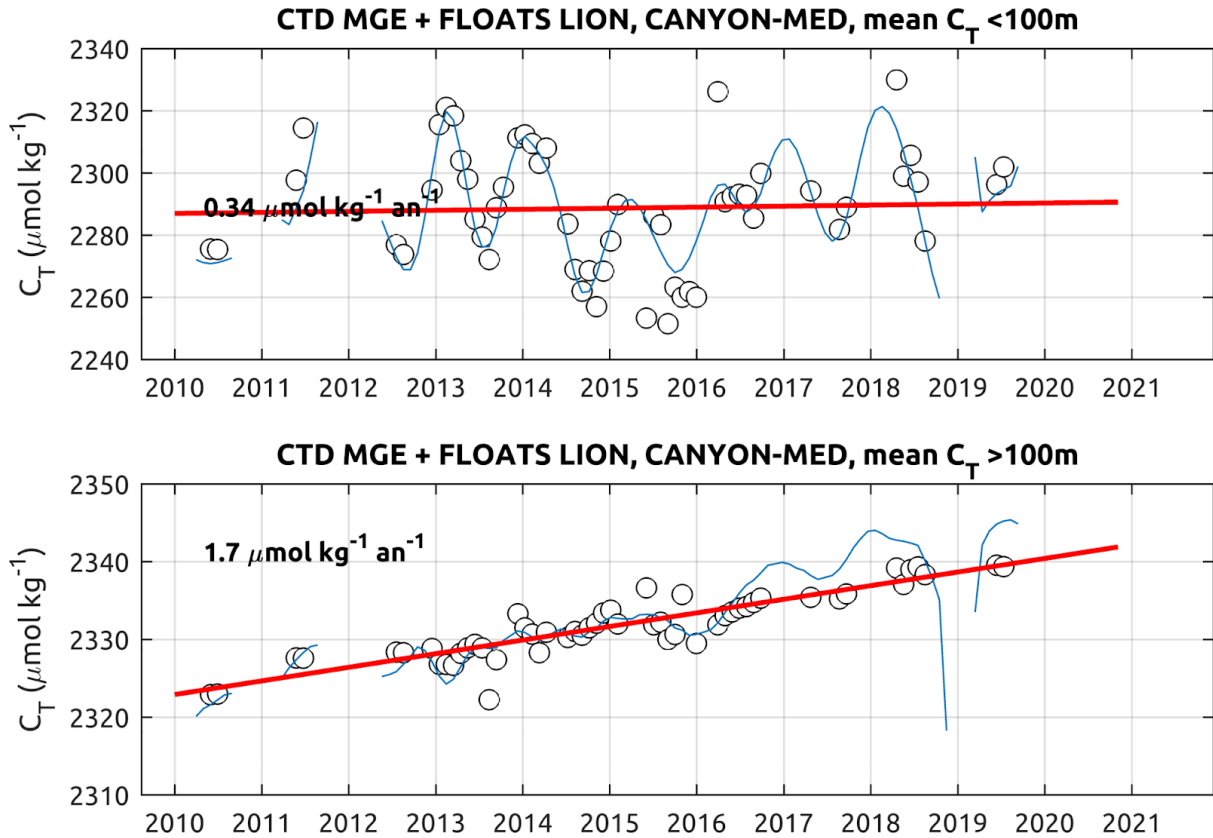


Figure 15. Trends in the mean DIC concentration ( $\mu\text{mol}/\text{kg}$ ) between 2010 and 2021 at the LION site in the upper water column (0-100dBar) (Top panel) and in the rest of the water column (100-2500 dBar).

In order to obtain more continuous estimates of DIC changes, CANYON-MED was applied to the entire fleet of float data equipped with O<sub>2</sub> sensors at the scale of two sub-region of the North Western Mediterranean Sea (Fourier et al., 2022). Over a seven-year period, none of the trends for carbonate system variables are significant in the upper water column surface, certainly due to the short period considered (DIC changes of less than 20  $\mu\text{mol.kg}^{-1}$  over 7 years are expected) compared to the strong seasonal variability (more than 100  $\mu\text{mol.kg}^{-1}$  over a seasonal cycle). In intermediate waters, results for DIC increased twice faster in intermediate waters than previously estimated (Coppola et al., 2020) while at depth the results were similar (Table 1). It should be noted that the trends at intermediate depths described by Coppola et al. (2020) spanned over the 300–800 m layer whereas Fourier et al. (2022) focused on the area around the O<sub>2</sub> minimum, therefore covering a smaller vertical portion. The distribution of DIC in the water column is driven by an equilibrium between the biological pump, which lowers DIC at the surface and increases it at intermediate depths, and the exchanges of CO<sub>2</sub> at the air-sea interface. Strong mixing events episodically bring together intermediate waters with cold surface waters poorer in Alkalinity and DIC, and depending on convection strength DIC-enriched deep waters as compared to the intermediate waters. The effect of intermittent deep convection events (not occurring every year) has therefore strong implications on the DIC accumulation at intermediate and deep levels because and could largely affect the trends of carbon accumulation in the water column.

Table 1. Estimates for Total Carbon changes in  $\mu\text{mol.kg}^{-1}$  for the Gulf of Lion (GOL) and the Ligurian Sea (LIG), extracted from Fourier et al. (2022)

Data Type	Area	period	Surface layer trend	Intermediate layer trend	Deep layer trend	Reference
CANYON-MED	GOL	2013-2020		2.73+/-0.60	1.20+/-0.39	Fourier et al. (2022)
CANYON-MED	LIG	2013-2020		2.56+/-1.31	1.60+/-1.13	Fourier et al. (2022)
Shipborne	LIG	1986-2016	0.59+/-0.34	1.18+/_0.09	1.36+/-0.16	Coppola et al. (2020)
Mooring	LIG	1995-1997 2013-2015	1.40+/-0.15			Merlivat et al. (2018)

## Anthropogenic carbon

In the Irminger Sea, the highest  $C_{ant}$  concentrations are located in the ocean surface and these values decrease with depth (Figure 16). Surface values reach  $\sim 55 \mu\text{mol/kg}$  in January 2011 and increase to  $70 \mu\text{mol/kg}$  in January 2022. These absolute values are in agreement with previous  $C_{ant}$  concentrations estimated via ship-based measurements (Zunino et al., 2014, Pérez et al., 2018). This change in surface  $C_{ant}$  concentration represents an increase of 27% during the whole study period. Taking as reference January 2011, surface  $C_{ant}$  represents 2.6% of surface DIC. The anthropogenic contribution to the total DIC pool increases throughout the period of observations, representing up to 3.2% in January 2022. At 1500 dbar,  $C_{ant}$  concentration reaches  $31 \mu\text{mol/kg}$  in January 2011 while this concentration increases to  $36 \mu\text{mol/kg}$  in January 2022. This increase is within the uncertainty range ( $\pm 5 \mu\text{mol/kg}$ ) of our computations, preventing any further analysis. The redistribution of  $C_{ant}$  at depth is mainly linked to oceanic circulation, water mass transformation and diffusion, therefore the associated timescales can be longer than those of the air-sea exchange ( $\leq 1$  year), explaining the stable  $C_{ant}$  concentration at depth compared to the increase in the ocean surface. The time-evolution of the iso  $C_{ant}$   $35 \mu\text{mol/kg}$  illustrates how  $C_{ant}$  deepens throughout the study period (Figure 16). This iso  $C_{ant}$  varies from  $\sim 900$  dbar in January 2011 to  $\sim 1400$  dbar in January 2022, indicating the progressive increase of  $C_{ant}$  at depth through time.

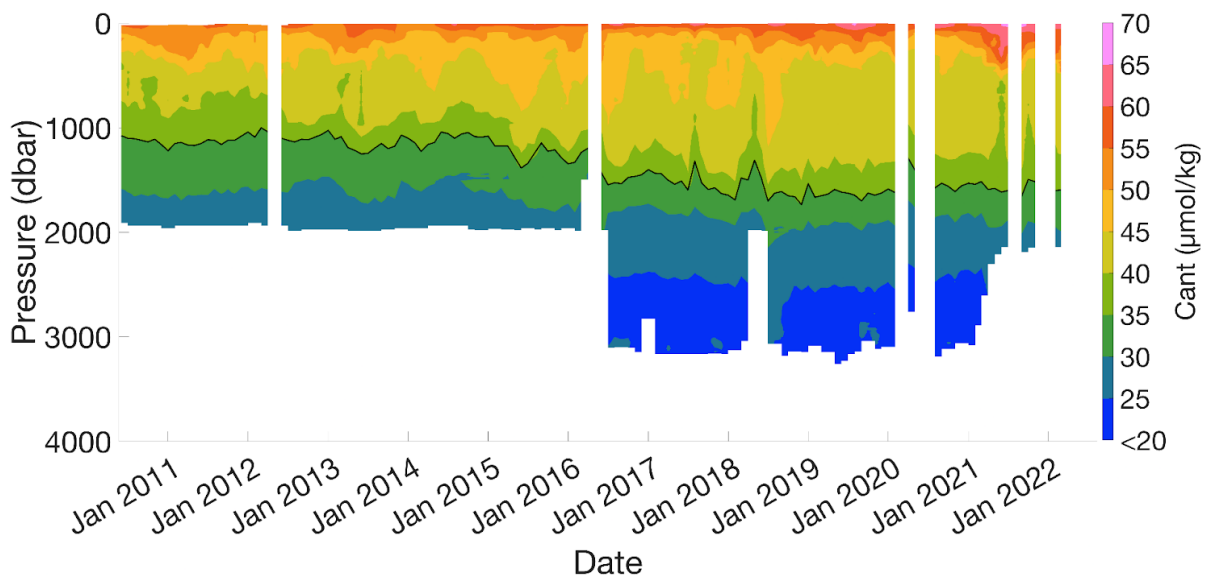


Figure 16. Distribution of anthropogenic carbon ( $\mu\text{mol/kg}$ ) in the Irminger Sea through time. The time-series have been averaged to obtain one  $C_{ant}$  profile per month. The black line represents the iso $C_{ant}$   $35 \mu\text{mol/kg}$ .

To further investigate the interannual to decadal variability of  $C_{ant}$  in the Irminger Sea, we divided the water column into several pressure layers (Figure 17). All the layers show a certain degree of interannual  $C_{ant}$  variability, with an overarching  $C_{ant}$  increase tendency present in all them. However, most of the  $C_{ant}$  fluctuations, especially for the first four years of the time series, remain within the mean  $\pm 5 \mu\text{mol/kg}$  uncertainty of the  $C_{ant}$  estimation method, preventing us from establishing clear interannual patterns. However, for certain periods and layers, the  $C_{ant}$  fluctuations are higher than the uncertainty range, permitting further analysis. The surface (0-300 dbar) layer experiences the largest  $C_{ant}$  fluctuations by the end of the study period, with an increase of  $8 \mu\text{mol/kg}$  between 2017 and 2021. The deeper layers (900-1200 dbar, 1200-1500 dbar and 1500-1800 dbar), however, show a decoupled pattern from the one described at the surface. The largest mean  $C_{ant}$  increase took place between 2014 and 2019. We relate this sharp deep

increase of  $C_{ant}$  increase with the intense convection activity in the Irminger Sea during this period (Zunino et al., 2020). Large convection events (intense ventilation) favours water-column homogenization and, hence, lead to a vertical direct transfer of  $C_{ant}$  from the upper oceanic layers towards the deeper layers.

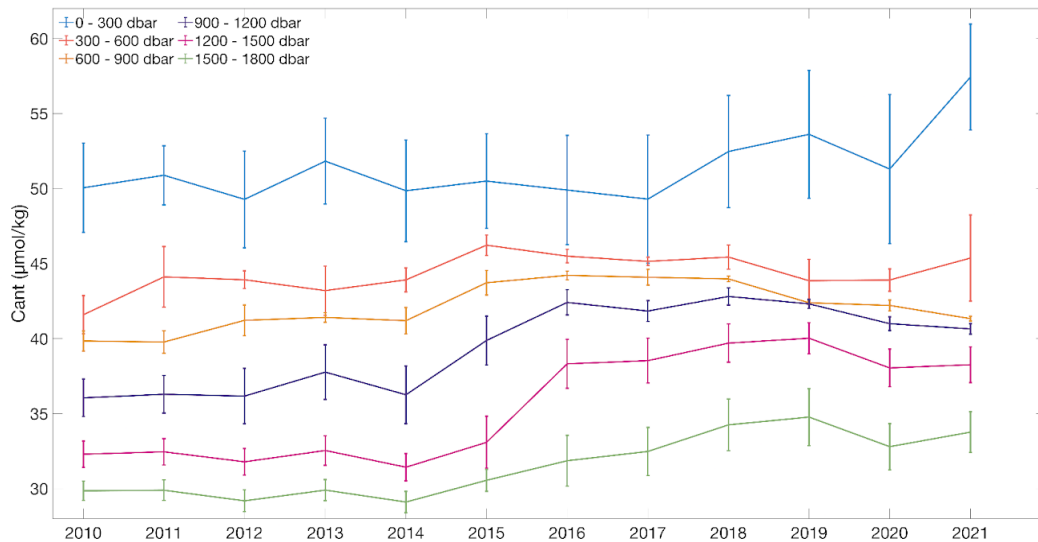


Figure 17. Interannual  $C_{ant}$  concentration ( $\mu\text{mol}/\text{kg}$ ) between 2010 and 2021. The water column is divided into 6 layers of 300 dbar.

We also assess the changes in the water-column  $C_{ant}$  inventory in the Irminger Sea between the surface and 1800 dbar (Figure 18). The  $C_{ant}$  inventories are calculated following the method of Pérez et al. (2010) and Raimondi et al. (2021), here applied to the Argo-NN-based  $C_{ant}$  data (Figure 18). Additionally, we calculate the  $C_{ant}$  storage rates, as the linear fitting to these  $C_{ant}$  inventory time series (Pérez et al., 2010; Fröb et al., 2018). Our results based on Argo data indicate that the  $C_{ant}$  inventory increased from 70 mol/m<sup>2</sup> in 2010 to 80 mol/m<sup>2</sup> in 2021. During this period, the  $C_{ant}$  storage rate is  $1.03 \pm 0.14$  mol/m<sup>2</sup>/yr. As demonstrated in previous studies (Pérez et al., 2010; Fröb et al., 2016; Fröb et al., 2018), our results confirm that the Irminger Basin is a region where  $C_{ant}$  inventory increases, proving the validity of our methodology to get such estimates. However, the existing discrepancies in the magnitude of the inventory among studies (Figure 18) are due to several factors. First, the magnitude of  $C_{ant}$  inventories are largely dependent of the data used to compute them (cruises section, e.g. Pérez et al., 2010, Fröb et al., 2016, 2018 vs full basin data, e.g. this study). Second it depends on the depth range taken into consideration (full water-column, Pérez et al. 2010, Fröb et al. 2016, 2018, vs 0-1800 dbar, this study). Third, it also depends on the method used to estimate  $C_{ant}$  ( $\phi\text{COT}$  method, e.g. Pérez et al., 2010, Fröb et al. 2018, this study, vs TTD method e.g. Fröb et al. 2016). Figure 9 also highlights the benefit of using Argo floats to increase the temporal coverage of  $C_{ant}$  data, compared to the more sparse and low temporal coverage of ship-based measurements of  $C_{ant}$  inventory (Pérez et al., 2010; Fröb et al., 2016; Fröb et al., 2018).

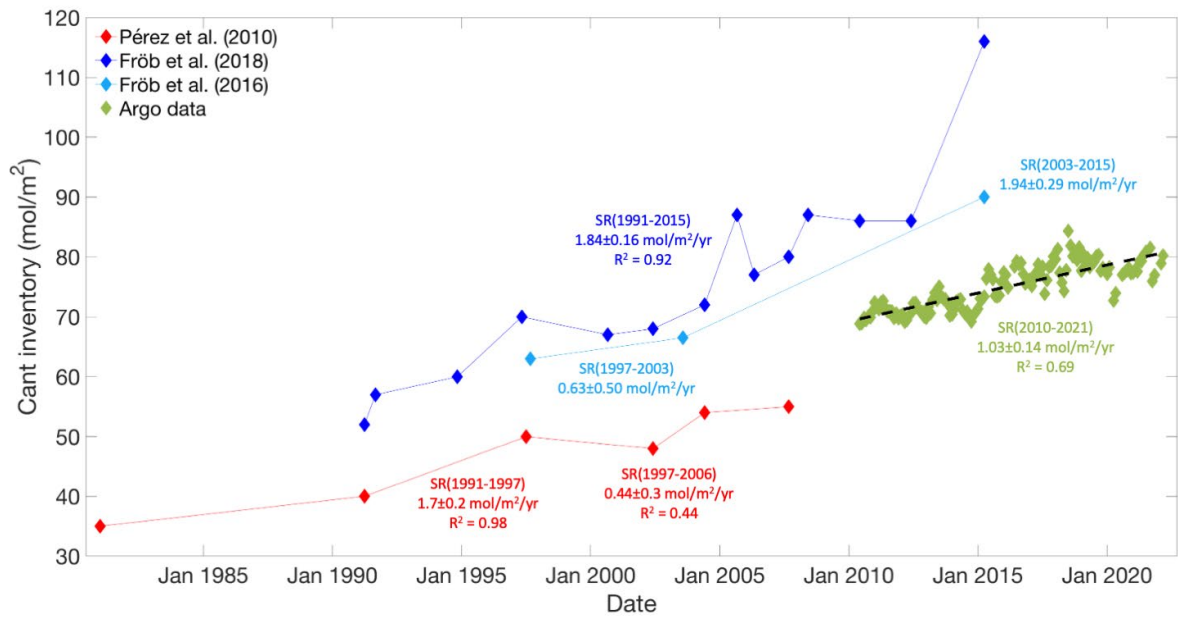


Figure 18. Anthropogenic carbon inventory ( $\text{mol}/\text{m}^2$ ) for the Irminger Sea.  $C_{\text{ant}}$  inventory from the Argo data are calculated with the  $\varphi\text{CoT}$  method (Pérez et al., 2008) from the surface until 1800 dbar.  $C_{\text{ant}}$  inventory from Pérez et al. (2010) are calculated with the  $\varphi\text{CoT}$  method (Pérez et al., 2008) along the whole water column.  $C_{\text{ant}}$  inventory from Fröb et al. (2018) are calculated with the  $\varphi\text{CoT}$  method (Pérez et al., 2008) along the whole water column.  $C_{\text{ant}}$  inventory from Fröb et al. (2016) are calculated with the TTD method (Vaugh et al., 2006) from the surface until 2000 dbar. SR = storage rate.

## Dissolved gases in the Deep Western Boundary Current

As reported in Koelling et al. (2022), two years of oxygen records from the 53°N observatory at the exit of the Labrador Sea (Figure 19) show already pronounced variations that can be interpreted as interannual variability. The variability also is visible across neighbouring moorings labelled here K7, K8, K9, K10 and covering the boundary current from most inshore (K7) to most offshore (K10) (Figure 2 in Koelling et al. (2022)). Although the time series is too short to come up with robust conclusions on the interannual variability it suggests that moored/stationary observations are key to interpret the temporal variability across the boundary current. Lagrangian observations (e.g., profiling floats) would most likely fail in recording the variability because they will drift quickly away in the fast-flowing boundary current.

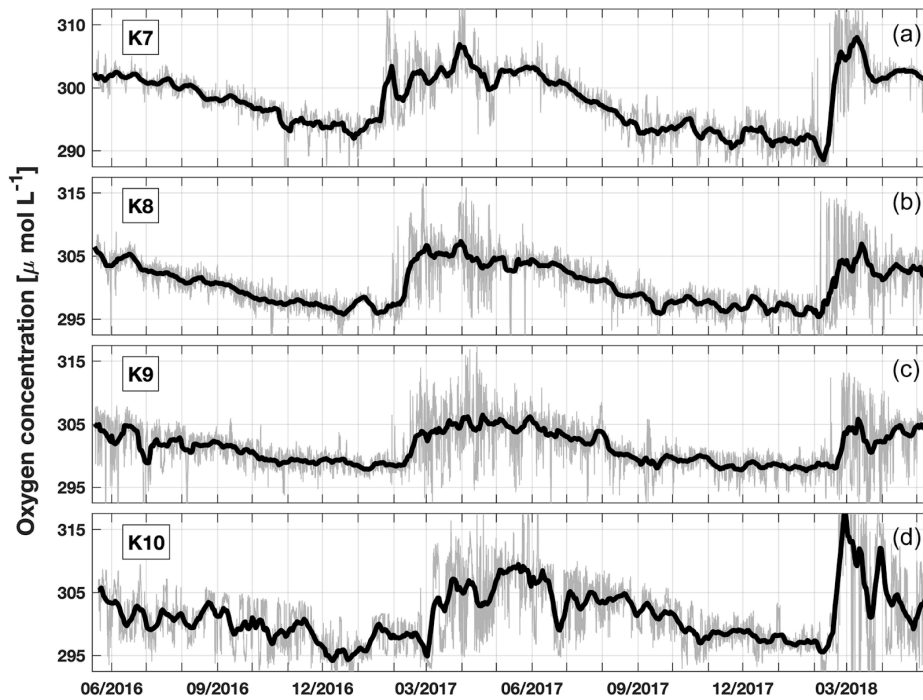


Figure 19. Time series of oxygen concentration at 610 m for K7, K8, K9, and K10 (a–d). Gray lines show original 15 min data, and black lines show time series filtered with a 10 d running mean. Note that axis limits are 5  $\mu\text{mol/l}$  lower in (a), but the range is the same for all panels (from Koelling et al. 2022).

### 3.3. Spatial variability

Of great interest is also the spatial extent of variability in carbon inventory changes and which very much is a prerequisite for the observational methods to apply. Clearly sampling has to consider the local Rossby radius as a natural scale of variability of ocean dynamics and in turn of biogeochemical (and ecosystem) processes that respond to for example upwelling driven productivity events.

The Argo-float-based study already discussed also describes the  $C_{\text{ant}}$  pathways towards the deep North Atlantic Ocean (Asselot et al. in prep). Most oceanic  $C_{\text{ant}}$  is absorbed in the subtropics where surface waters are characterized by a low Revelle factor (Revelle & Suess, 1957). These waters with a low Revelle factor uptake large amount of  $C_{\text{ant}}$  from the atmosphere. The North Atlantic Central Water (NACW), situated near Newfoundland, is known to carry subtropical waters and is therefore characterized by high concentrations of  $C_{\text{ant}}$ . Indeed, between the surface and 400 dbar, the average concentration of  $C_{\text{ant}}$  in the NACW is 61  $\mu\text{mol/kg}$  (Figure 20). The North Atlantic Current (NAC), flowing from the subtropics to the subpolar gyre, transports the NACW with high  $C_{\text{ant}}$  concentrations towards the Iceland Basin. This particular basin is characterized by the presence of Subpolar Mode Water (SPMW) that is formed during winter convection by intense air-sea buoyancy loss, leading to the densification of the  $C_{\text{ant}}$ -loaded NACW on its way towards subpolar latitudes (Brambilla et al., 2008; Brambilla and Talley, 2008). As a consequence, in the first 600 dbar, the SPMW are characterized by an average  $C_{\text{ant}}$  concentration of 53  $\mu\text{mol/kg}$  (Figure 21 and Figure 22). This result highlights a first deepening of  $C_{\text{ant}}$  between the Newfoundland basin and the Iceland Basin due to the formation of SPMW. Following the anticyclonic circulation pathway above the Reykjanes Ridge, the SPMW fades away above the ridge, leading to a dilution and substantial deepening of  $C_{\text{ant}}$  in the Irminger Sea (Figure 21 and Figure 22). This wide  $C_{\text{ant}}$  deepening above the Reykjanes Ridge is due to the densification of the ocean surface where surface  $C_{\text{ant}}$ -loaded waters are going into the deep ocean. As a consequence, maximum  $C_{\text{ant}}$

concentrations of  $40 \mu\text{mol/kg}$  are found as deep as 1200 dbar in the Irminger Sea. Furthermore, these large  $C_{\text{ant}}$  concentrations are constrained within the Labrador Sea Water (LSW), meaning that the formation of this particular water mass traps  $C_{\text{ant}}$  and brings it into the deep ocean. Following the general circulation patterns,  $C_{\text{ant}}$  is transported out of the Irminger Sea by the Western Boundary Current and arrives in the Labrador Sea. In this particular basin, maximum  $C_{\text{ant}}$  concentrations of  $40 \mu\text{mol/kg}$  are located at pressure levels of 1600 dbar (Figure 20 and Figure 21). As in the Irminger Sea, high  $C_{\text{ant}}$  concentrations are trapped within the LSW. The densification of this water mass transports  $C_{\text{ant}}$  towards the deep North Atlantic Ocean. Once formed, LSW spreads along three major pathways (Talley & McCartney, 1982), carrying  $C_{\text{ant}}$  all over the North Atlantic Ocean. First, it flows southward as part of the Deep Western Boundary Current, leading to a deep transfer of  $C_{\text{ant}}$  from the subpolar gyre to the subtropics. Second, this water mass flows eastward below the NACW, transporting waters with maximum  $C_{\text{ant}}$  concentrations of  $\sim 35 \mu\text{mol/kg}$  (Figure 20). Third, LSW flows north-eastward directly into the Irminger Sea, trapping  $C_{\text{ant}}$  signal in the deep levels of the subpolar North Atlantic gyre.

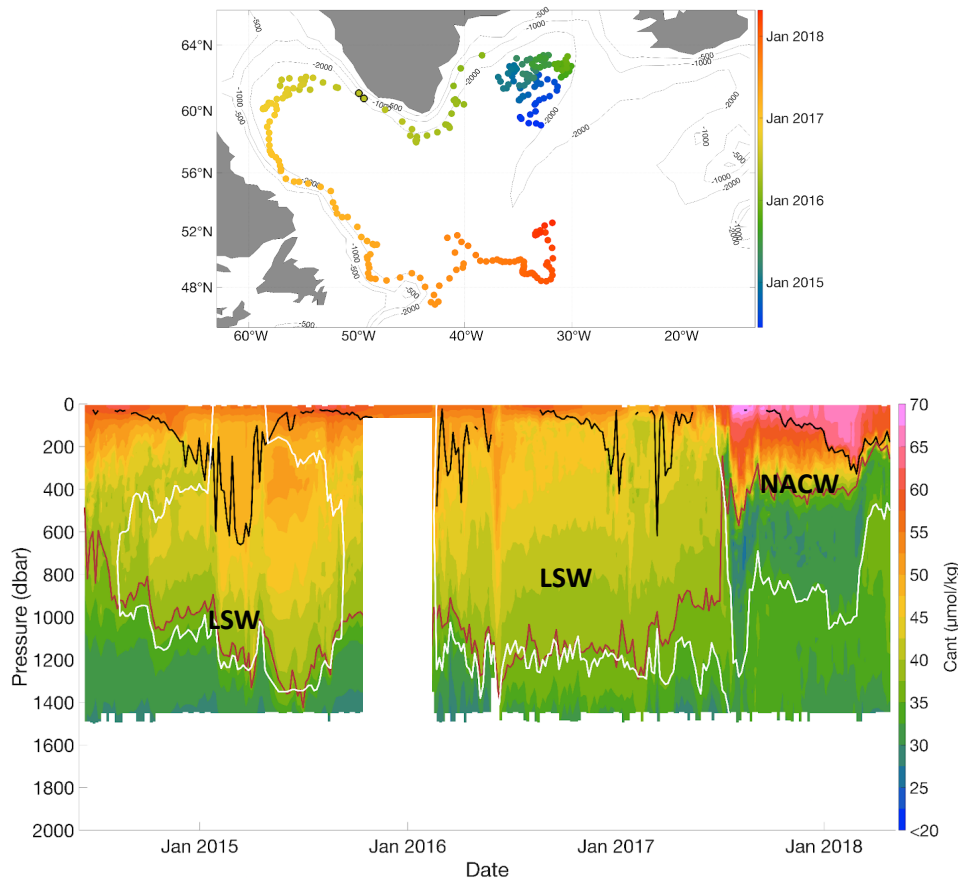


Figure 20. Top panel: Trajectory of the Argo float 5904988. The color represents the date with blue being the beginning of the trajectory and red being the end. Bottom panel:  $C_{\text{ant}}$  section along the float trajectory. The black line represents the MLD. The white lines represent the limits of the LSW, defined by oxygen greater than  $290 \mu\text{mol/kg}$  in the Labrador and Irminger Seas and salinity lower than 34.94 outside these two basins. The brown line represents the  $\text{iso}C_{\text{ant}} 37 \mu\text{mol/kg}$ . Source: Asselot et al. (in prep).

To summarize, the deepening of  $C_{\text{ant}}$  along its journey through the subpolar North Atlantic gyre is divided in four steps. First,  $C_{\text{ant}}$  uptake from the atmosphere in the subtropics is transported by the NAC where it is constrained in the NACW and reaches pressure levels of 400 dbar. Second, the formation of the SPMWs in

the Iceland Basin leads to a deepening of  $C_{ant}$  until 600 dbar. Third, the Reykjanes Ridge acts as a physical barrier where  $C_{ant}$  signal deepens into the Irminger Sea and the high  $C_{ant}$  concentrations are found as deep as 1400 dbar in this basin. Fourth, in the Labrador Sea, high  $C_{ant}$  concentrations can be found as deep as 1600 dbar due to the formation of the LSW. The formation of this particular water mass leads also to the transport of  $C_{ant}$  out of the subpolar North Atlantic gyre.

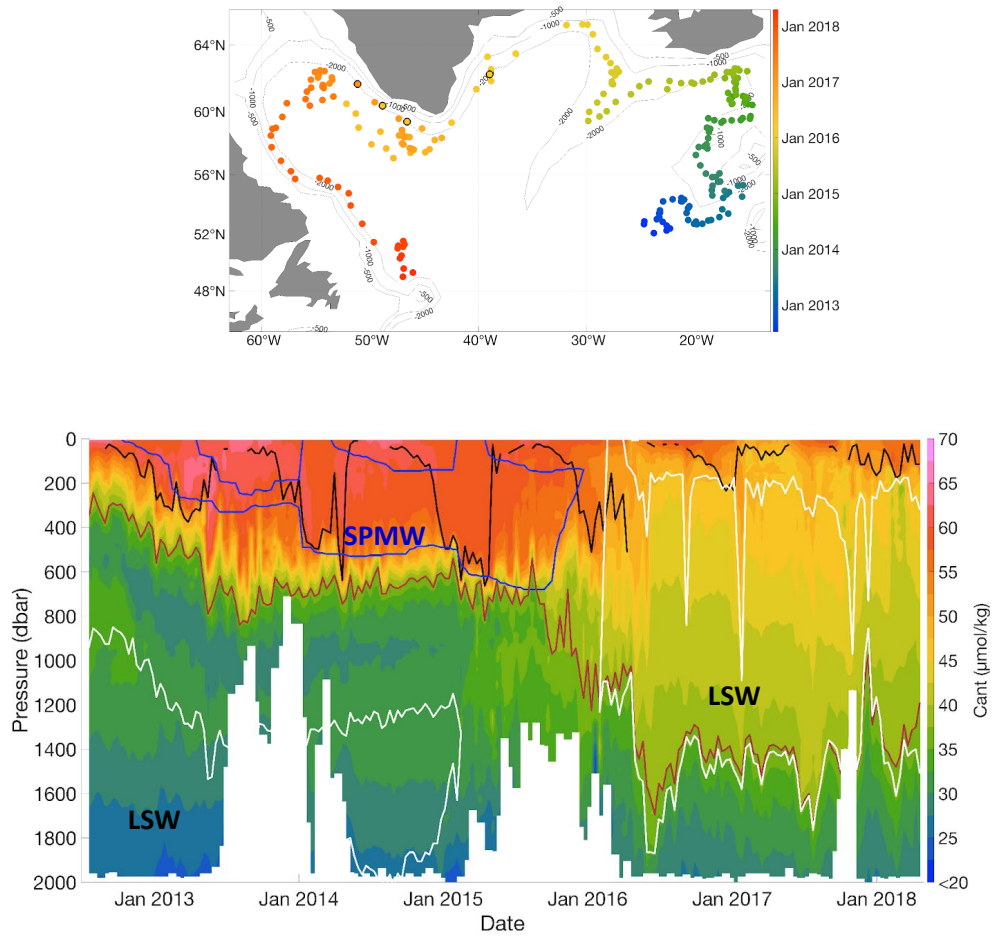


Figure 21. Top panel: Trajectory of the Argo float 6901023. The color represents the date with blue being the beginning of the trajectory and red being the end. Bottom panel:  $C_{ant}$  section along the float trajectory. The black line represents the MLD. The white lines represent the limits of the LSW, defined by oxygen greater than  $290 \mu\text{mol/kg}$  in the Labrador and Irminger Seas and salinity lower than 34.94 outside these two basins. The blue lines represent the limits of the SPMW defined by a potential vorticity lower than  $6 \times 10^{-11} \text{ m}^{-1} \text{ s}^{-1}$ . The brown line represents the iso $C_{ant}$   $37 \mu\text{mol/kg}$ . Source: Asselot et al. (in prep).

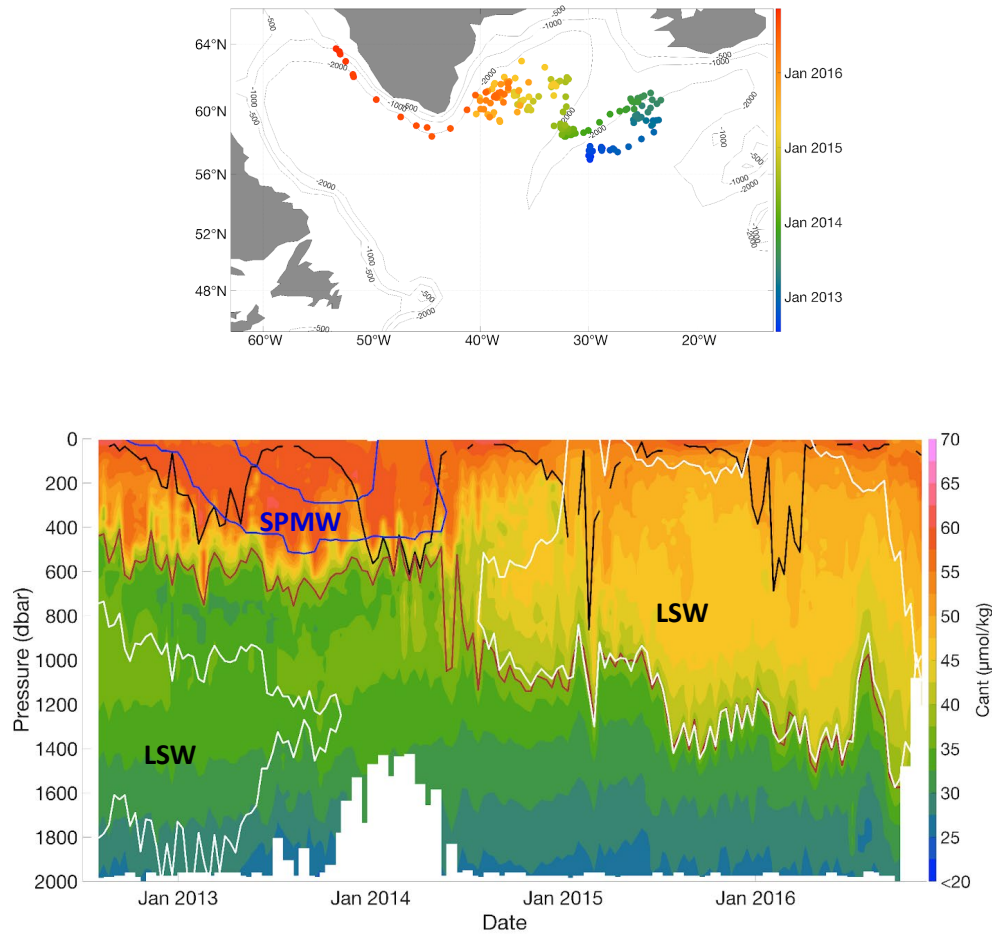


Figure 22. Top panel: Trajectory of the Argo float 6901026. The color represents the date with blue being the beginning of the trajectory and red being the end. Bottom panel:  $C_{ant}$  section along the float trajectory. The black line represents the MLD. The white lines represent the limits of the LSW, defined by oxygen greater than  $290 \mu\text{mol/kg}$  in the Labrador and Irminger Seas and salinity lower than 34.94 outside these two basins. The blue lines represent the limits of the SPMW defined by a potential vorticity lower than  $6 \times 10^{-11} \text{ m}^{-1} \text{ s}^{-1}$ . The brown line represents the iso $C_{ant}$   $37 \mu\text{mol/kg}$ . Source: Asselot et al. (in prep).

Although of interest is to better define the pattern of carbon uptake at the sea surface for example as being represented by the  $p\text{CO}_2$  field. In terms of observations,  $p\text{CO}_2$  is observed mostly by analysis systems installed on ships and that analyse the seawater intake with high accuracy and based on reference material (Steinhoff et al. 2019). In order to generate maps of the  $p\text{CO}_2$  concentration a data homogenization and quality control is required and in turn the “along track” data, which is very heterogeneous, can be mapped, often via objective mapping techniques. A new approach (Olivier et al. 2022) was applied to a very rich co-located multiparameter data set acquired in the framework of the EUREC4A-OA/ATOMIC campaign that was executed in the northwestern tropical Atlantic and which provided for the first-time synoptic measurements of winter air–sea fluxes of  $\text{CO}_2$  in that region. By making use of a statistical approach that created relationships between ship-measured parameters that are also accessible from satellite remote sensing (sea surface temperature, salinity, and chlorophyll) and  $p\text{CO}_2$ . This way, a high resolution  $p\text{CO}_2$  map could be generated for this particular period that illustrates how rich in structures the surface  $p\text{CO}_2$  field and hence also the  $\text{CO}_2$ -flux field may look, and which is strikingly different from maps based on objective mapping of

sparse pCO<sub>2</sub> data only (Figure 23). By adding the local, western Tropical Atlantic Exclusive Economic Zones (EEZ) of the neighbouring countries, the potential impact of the spatial sampling on surface carbon flux for EEZ assessments is evident. Qualitatively, it is easy to see that the resolution can have potentially dramatic consequences for individual EEZ regions, up to a reversal from a CO<sub>2</sub> source to a CO<sub>2</sub> sink.

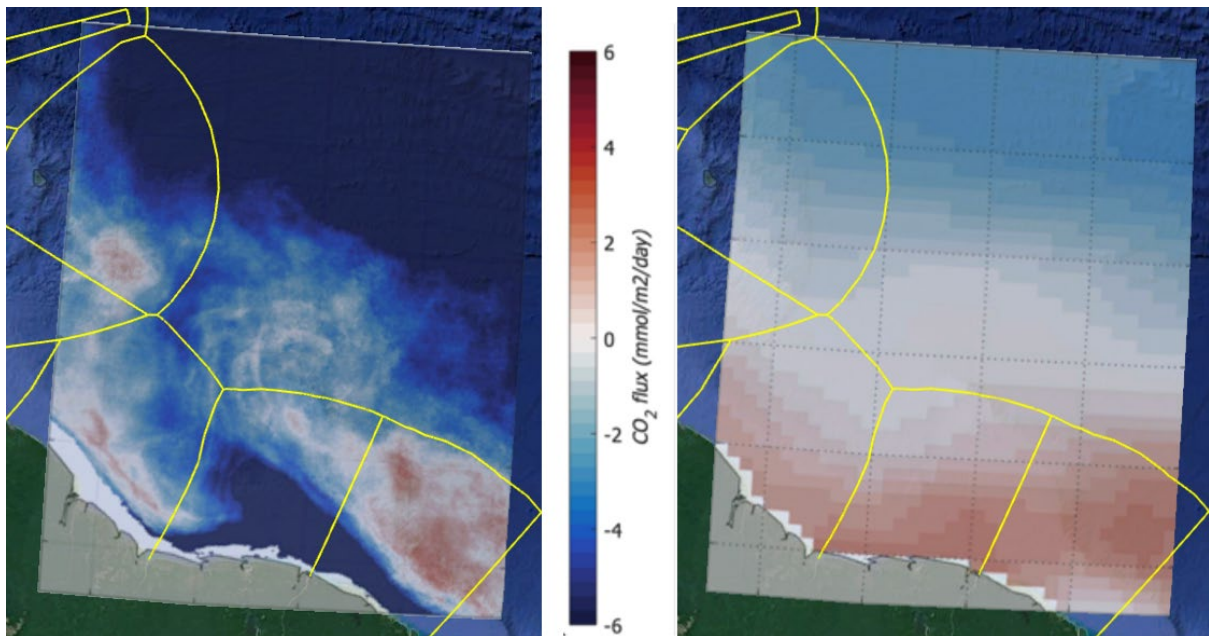


Figure 23. (left) Jan/Feb 2020 surface CO<sub>2</sub> flux map for the western Tropical Atlantic after Olivier et al. (2022), (right) Long term mean flux as estimated in Landschützer et al. 2020). The yellow lines in both maps show the approximate boundaries of local EEZ regions.

### 3.4. Quantitative aspects through modelling

The annual budget of dissolved inorganic carbon in the deep convection area of the northwestern Mediterranean Sea has been investigated over the period September 2012 to September 2013, using a 3-dimensional coupled physical-biogeochemical-chemical modelling approach. This year was particularly rich in observations thanks to the DEWEX experiment and the MOOSE-GE yearly cruises. An accurate setup and validation of the coupled model was possible thanks to 5 cruises at the scale of the North Western Mediterranean and the massive deployment of O<sub>2</sub>-equipped Argo Floats and the monthly profiles carried out at DYFAMED and BOUSSOLE sites (Ulses et al, in rev.).

The model outputs allowed us to investigate the fluxes of DIC in a 3-dimensional way. The maxima of the lateral DIC transport in the upper layer of the water column averaged over the whole winter period are found in the general circulation, especially in the Northern Current, the Balearic Current and the Balearic Front, separating the southern less salty Atlantic waters from the deep convection salty waters (Figure 24a and Figure 24c). The instabilities developing at the periphery of the deep convection area favoured the incorporation of saltier and DIC-enriched waters in the general circulation through a bleeding effect, similarly as described by Herrmann et al. (2008) for the export of newly-formed dense waters from the deep convection area, (i) at the western boundaries of the deep convection area towards the Balearic Sea, and towards the Algerian basin by the southern extension of the Balearic Current, as well as (ii) along the Balearic Front between the Minorca Balearic Island and Corsica, as illustrated in Figure 24c and Figure 24d. Finally,

Figure 24b shows that the vertical DIC supply into the upper layer during winter resulted from upward and downward vertical fluxes of small scales due to the absence of stratification.

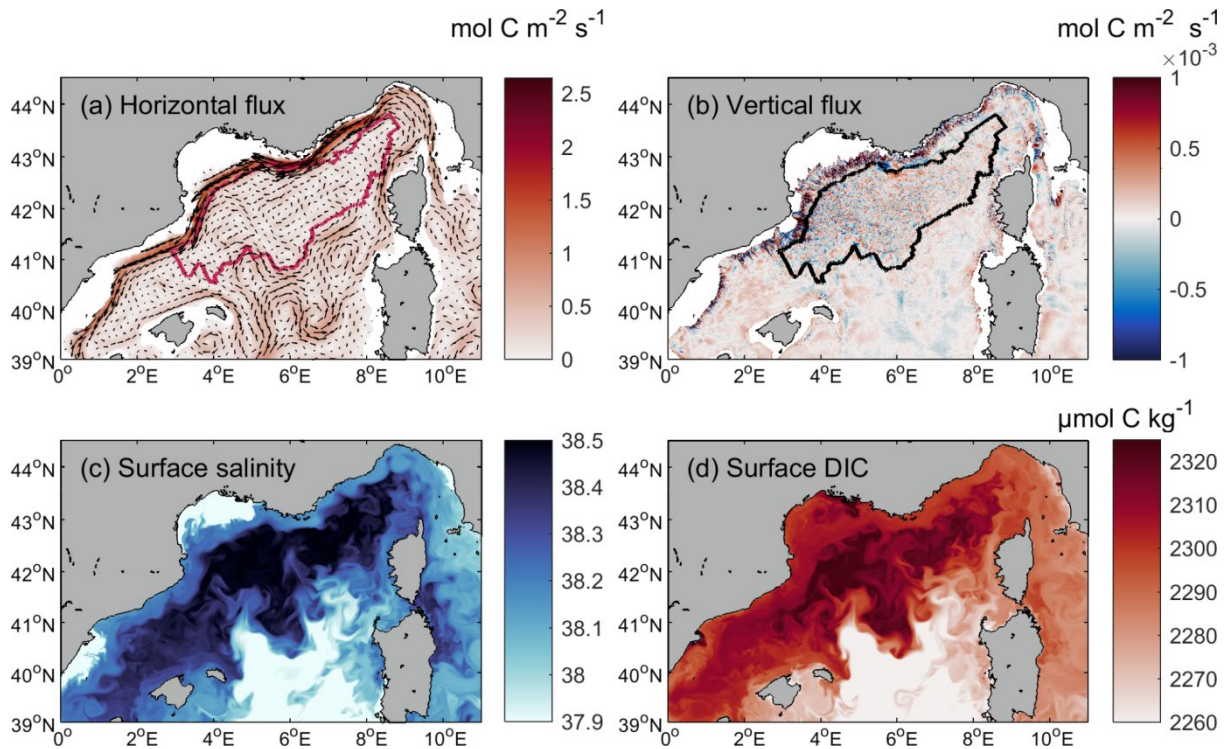


Figure 24. (a) Winter horizontal flux of dissolved inorganic carbon (DIC,  $\text{mol C m}^{-2} \text{ s}^{-1}$ ), vertically integrated over the upper layer (0–150 m), (b) winter vertical DIC flux ( $\text{mol C m}^{-2} \text{ s}^{-1}$ ) at 150 m, (c) surface salinity and (d) DIC concentration ( $\mu\text{mol C kg}^{-1}$ ) on 4 March 2013. (From Ulses et al. in rev.).

Our results show that both biological and physical processes dominate the CO<sub>2</sub> budget in the upper layer (0–150 m) of the convection zone for the study period. Through their impacts on DIC concentration, biological and physical flows have both a major role in the intensity and sign of the air-sea exchanges in the deep convection area.

Figure 25 shows a schematic of the annual budget of dissolved inorganic carbon in the deep convection zone. Our model results show that the deep convection area acted as a moderate CO<sub>2</sub> sink for the atmosphere on an annual scale, over the period September 2012–September 2013. We estimate that it absorbed 0.5 mol C m<sup>-2</sup> of atmospheric CO<sub>2</sub>. This uptake of atmospheric CO<sub>2</sub> displayed spatial variability (Figure 26). It was greater than 1 mol C m<sup>-2</sup> in the northern edge of the area along the Northern Current flowing over the Gulf of Lion continental slope, and became less than 0.25 mol C m<sup>-2</sup> in the western and eastern edge areas. One can notice that the annual rate remained lower than on the Gulf of Lion’s shelf, which is beyond the scope of this study. Within the sea, biogeochemical processes induced an annual consumption of 3.7 mol C m of DIC in the upper layer and a production of 2.3 mol C m in the deeper layers. The deep convection area thus appears as a net autotrophic region from a biological point of view, with a DIC consumption of 1.5 mol C m considering the whole water column.

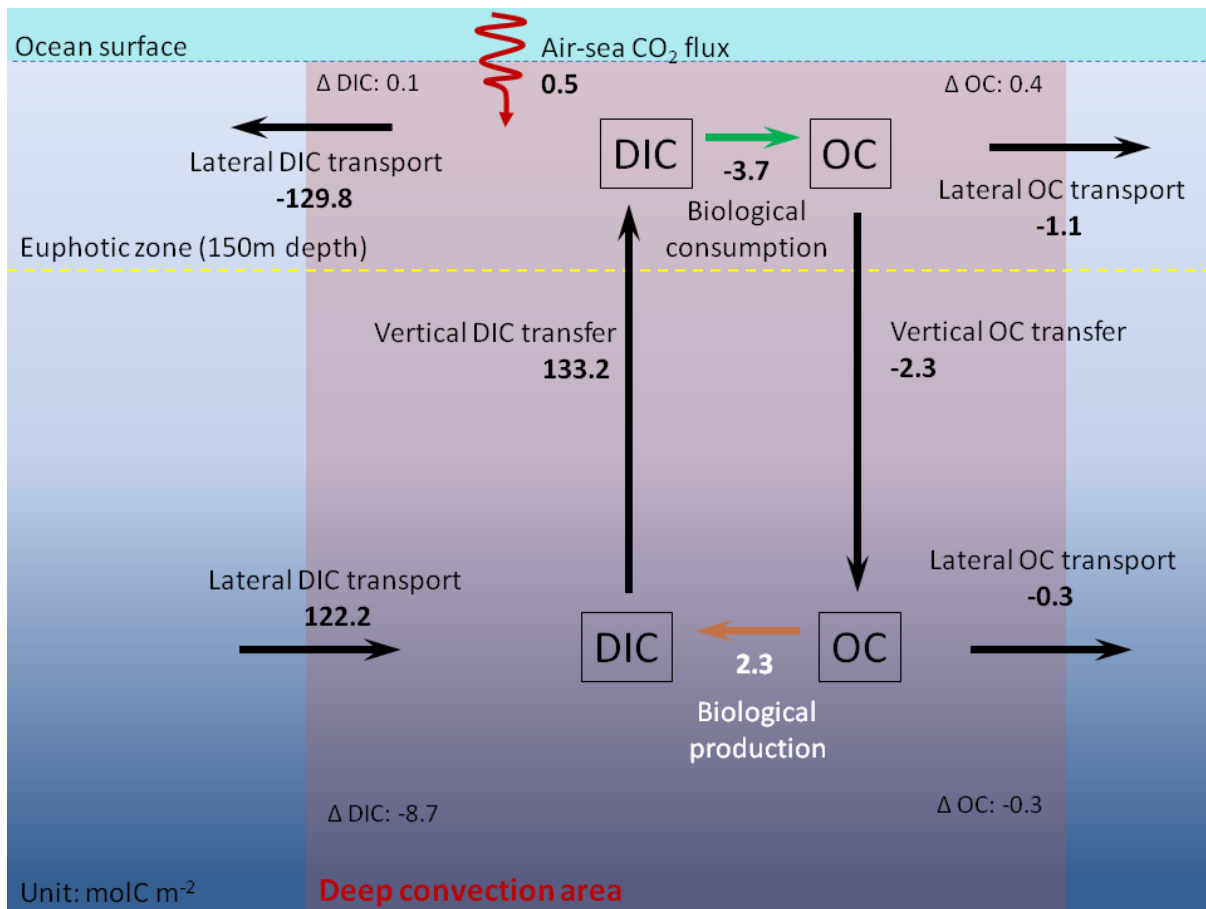


Figure 25. Scheme of the carbon budget for the period September 2012 to September 2013 from the coupled model SYMPHONIE-Eco3M-S. (From Ulses et al., in rev).

Our estimate of net physical fluxes (lateral plus vertical) is 3.3 mol C m in the upper layer and -11.0 mol C m in the deeper layer. Specifically, the model indicates a vertical DIC supply of 133.2 mol C m from the deeper layer to the upper layer, partly offset by a lateral outflow of 129.8 mol C m<sup>-2</sup> in the upper layer and an inflow of 122.2 mol C m<sup>-2</sup> in the deeper layer. The budget in the deep layer masks different signs of physical fluxes: if the deeper layer is subdivided into an intermediate layer (150 m-800 m) and the deeper most layer (800 m-bottom), we find that the former, the intermediate layer, gained an amount of 83.1 mol C m<sup>-2</sup> of DIC through vertical transport, while it lost 87.6 mol C m<sup>-2</sup> of DIC through lateral export. Finally, our model shows that the convection zone was a source of DIC of 8.7 mol C m<sup>-2</sup> for the rest of the western Mediterranean Sea. While the DIC inventory in the upper layer remained stable (decrease of 0.07 mol C m<sup>-2</sup>), the DIC inventory in the deeper layer experienced a decrease of 8.7 mol C m<sup>-2</sup>. This loss occurred mainly during deep convection, and to a lesser extent during the preconditioning period (in autumn and early winter).

Finally, we complete the inorganic carbon budget with the labile organic carbon fluxes (refractory organic carbon is not considered in our model). We estimate that during the studied period a lateral export of organic carbon of 1.1 mol C m<sup>-2</sup> and 0.3 mol C m<sup>-2</sup> took place in the upper and deeper layers, respectively. The modeled downward export of organic carbon amounted to 2.3 mol C m<sup>-2</sup>.

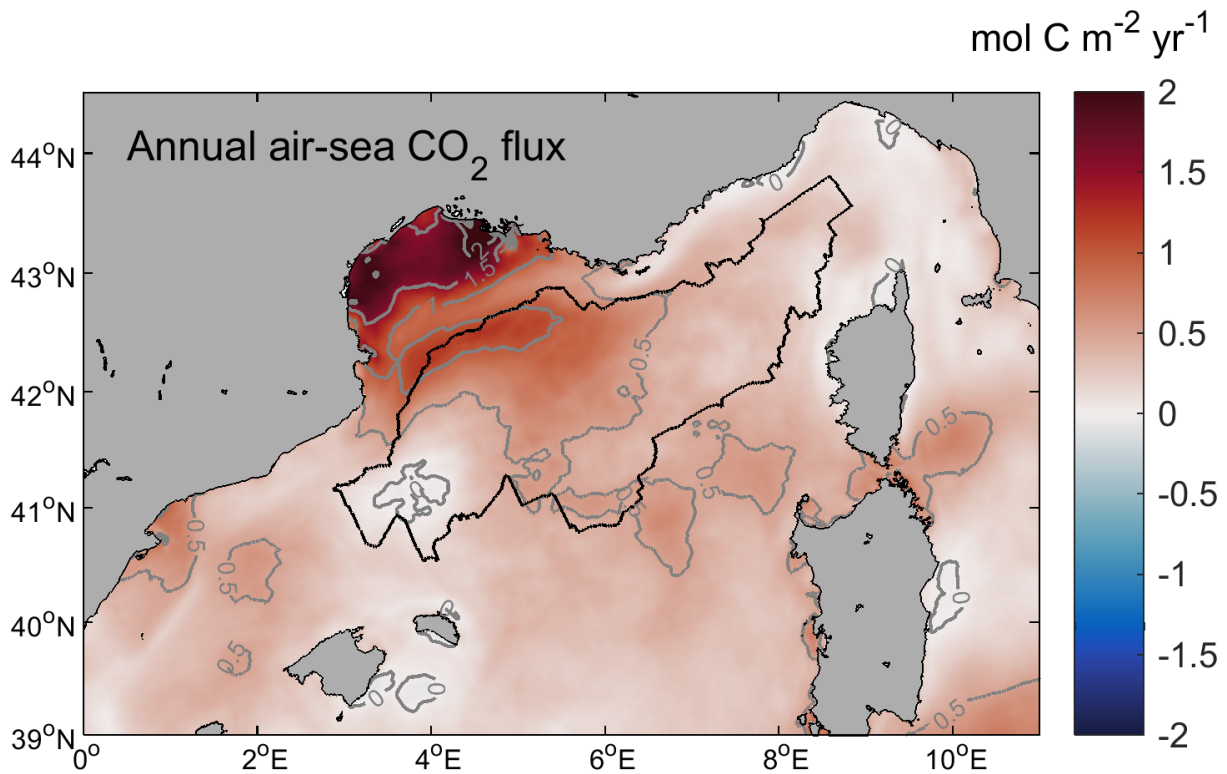


Figure 26. Modelled annual air-to-sea CO<sub>2</sub> flux (mol C m<sup>-2</sup> yr<sup>-1</sup>), averaged over the period September 2012-September 2013. The deep convection area is indicated by a black line. From Ulses et al. in rev.

We estimate that the northwestern Mediterranean Sea deep convection region was a moderate sink of CO<sub>2</sub> for the atmosphere over the study period (Figure 26). The model results show the reduction of CO<sub>2</sub> uptake during deep convection, and its increase during the abrupt spring phytoplankton bloom following the deep convection events. We highlight the dominant role of both biological and physical flows in the annual dissolved inorganic carbon budget. The upper layer of the northwestern deep convection region gained dissolved inorganic carbon through vertical physical supplies and, to a lesser extent, air-sea flux, and lost dissolved inorganic carbon through lateral transport and biological fluxes. The region, covering 2.5 % of the Mediterranean, acted as a source of dissolved inorganic carbon for the surface and intermediate water masses of the western and southern Western Mediterranean Sea and could contribute up to 10 and 20% to the CO<sub>2</sub> exchanges with the Eastern Mediterranean Sea and the Atlantic Ocean.

## 4. Conclusion and global implications

In this deliverable we present the work of EuroSea Task 7.1 focused on analysing the seasonal, multiannual and spatial variability of carbon in two major convection regions, Irminger and Labrador Sea for the North Atlantic, and Gulf of Lion for the Mediterranean Sea. The focus here is on dissolved inorganic carbon (DIC) and this also includes the anthropogenic signal in the DIC. The overarching objective is to narrow down the spread of quantification of the expected range of natural DIC variability. Knowing the range of natural DIC variability will enable estimating the signal to noise ratio for interior ocean carbon variability, which in turn will enable an assessment of the usability of the DIC variability in the global carbon stocktake process, which is the main motivation for EuroSea Task 7.1.

The work makes use of different approaches to derive DIC fields: on the one side the DIC is directly observed by chemical analysis of discrete bottle samples collected during ship expeditions (e.g., GO-SHIP cruises, national cruises). This data is considered of highest (known) quality, and builds the database for direct analysis, and is also used as the reference set for other approaches that can increase the coverage of DIC estimates. We actually need higher resolution carbon data sets than the ship-based observations in the context of carbon auditing at the EEZ level, in order to describe the carbon distributions at this scale. One such approach is using artificial neural networks/multiple-regression techniques which are applied to the high-quality ship data (e.g. using nutrient, oxygen, and hydrographic data) to derive empirical relations of non-carbon variables with DIC (total and anthropogenic). Having determined such empirical relations enables using these non-carbon data (hydrography, oxygen) to convert to DIC. Verification of the data is done by applying the empirical relations to the reference pool. Here it already becomes apparent that the sampling strategy of the high-quality data (e.g., resolving the seasonal cycle, sampling in various multiparameter regimes) is key for the expected accuracy of the reconstructed DIC. This work also highlights the complementary nature of the different components of the Global Ocean Observing System (GO-SHIP cruises, autonomous platforms) and the need to sustain all of them in the long-term to enable determination of new empirical relations in a changing ocean.

Our results describe the DIC variability and trends over the past years in the ocean interior in both the North Atlantic Ocean and the Mediterranean Sea, as well as the strong interplay of natural and anthropogenic signals in the long term. These will be important to consider, particularly when aiming for a more regional carbon auditing such as at the EEZ level. Both impact the oceanic carbon uptake, whose assessment is one of the remaining biggest challenges in climate science. The research presented here has provided fundamental advances in that respect.

We demonstrated that the combined use of high-quality data from cruises and DIC estimates from neural networks applied to autonomous platform data also allows for a better assessment of the performance of physical-biogeochemical numerical models and allows for fine-tuning them with respect to the DIC variability. Having confidence in the model realism both on the physical and biogeochemical aspects, we can use the modelled fields of carbon stocks and fluxes in a comprehensive way - an approach that should be considered more generally in the framework of carbon auditing at the EEZ level. A next important step would be to apply such an analysis at EEZ level (considering the coastal shallow area of the Gulf of Lion which appears to be a stronger carbon sink than the only deep convection area we have studied here). Such a study would also allow to elaborate on the advective processes which would link carbon uptake and variability from one national zone to another which can make the attribution of carbon uptake by EEZ a challenging problem. We

recommend further modelling studies using this methodology on the interannual scale not only in the Mediterranean Sea but also in other required areas for carbon auditing at the EEZ level.

We have shown that we cannot only consider the surface in the context of carbon auditing at the EEZ level but need to include the ocean interior carbon inventory and fluxes at the EEZs boundaries (surface and lateral). We have also demonstrated that we need to increase the space and time coverages of DIC estimates to make such inventories in that carbon auditing at the EEZ level context. To do so, we strongly recommend the use of DIC estimates by subsurface autonomous platforms and neural network techniques. It should be maintained and furthermore, generalised at the European and global scales. Our results have shown the strong skill of the neural network technique both in the North Atlantic Ocean and in the Mediterranean Sea but a key aspect is that the number and distribution of O<sub>2</sub>-equipped autonomous platforms must ensure that the spatial and temporal coverages are sufficient to describe the DIC variability. When considering a carbon audit at the EEZ level, this must be ensured in all the required areas and accompanied by surveys of high-quality ship-based co-located multiparameter data that is traceable to some type of reference material. They are key for direct analysis as well as it is for any multiparameter regression technique (linear, neural network, numerical modelling). The surveys shall be designed to cover the full and relevant multiparameter space, and also the relevant spatial and time scales to avoid aliasing effect in the baseline data. Specific observing system design experiments to better quantify our observational needs, at surface and in the ocean interior, would be needed in the future, in support of carbon auditing at the EEZ level.

## References

- Asselot, R., Carracedo, L.I., Thierry, V., et al. (in prep). Argo-O2 floats reveal the anthropogenic carbon pathways to the deep North Atlantic.
- Atamanchuk, D., J. Palter, H. Palevsky, I. Le Bras, J. Koelling, and D. Nicholson (2021). Linking oxygen and carbon uptake with the meridional overturning circulation using a transport mooring array. P. 9 in *Frontiers in Ocean Observing: Documenting Ecosystems, Understanding Environmental Changes, Forecasting Hazards*. E.S. Kappel, S.K. Juniper, S. Seeyave, E. Smith, and M. Visbeck, eds, *A Supplement to Oceanography* 34(4), <https://doi.org/10.5670/oceanog.2021.supplement.02-03>.
- Béthoux, J. P., De Madron, X. D., Nyffeler, F., & Tailliez, D. (2002). Deep water in the western Mediterranean: peculiar 1999 and 2000 characteristics, shelf formation hypothesis, variability since 1970 and geochemical inferences. *Journal of Marine Systems*, 33, 117-131.
- Bittig, H. C., Körtzinger, A., Neill, C., van Ooijen, E., Plant, J. N., Hahn, J., et al. (2018a). Oxygen Optode sensors: principle, characterization, calibration, and application in the ocean. *Front. Mar. Sci.* 4:429. doi: 10.3389/fmars.2017.00429
- Bittig, H.C., Steinhoff, T., Claustre, H., et al. (2018b). An alternative to static climatologies: Robust estimation of open ocean CO<sub>2</sub> variables and nutrient concentrations from T, S, and O<sub>2</sub> data using Bayesian neural networks. *Frontiers in Marine Science*, 5, 328.
- Brambilla, E., Talley, L.D., & Robbins, P.E. (2008). Subpolar mode water in the northeastern Atlantic: 2. Origin and transformation. *Journal of Geophysical Research: Oceans*, 113(C4).
- Brambilla, E., & Talley, L.D. (2008). Subpolar Mode Water in the northeastern Atlantic: 1. Averaged properties and mean circulation. *Journal of Geophysical Research: Oceans*, 113(C4).
- Carter, B.R., Bittig, H.C., Fassbender, A.J., et al. (2021). New and updated global empirical seawater property estimation routines. *Limnology and Oceanography: Methods*, 19(12), 785-809.
- Coppola, L., Legendre, L., Lefevre, D., et al. (2018). Seasonal and inter-annual variations of dissolved oxygen in the northwestern Mediterranean Sea (DYFAMED site). *Progress in Oceanography*, 162, 187-201.
- Coppola, L., Boutin, J., Gattuso, J.P., et al. (2020). The carbonate system in the Ligurian Sea. *The Mediterranean Sea in the Era of Global Change 1: 30 Years of Multidisciplinary Study of the Ligurian Sea*, 79-103.
- Davila, X., Gebbie, G., Brakstad, A., et al. (2022). How is the ocean anthropogenic carbon reservoir filled?. *Global Biogeochemical Cycles*, 36(5), e2021GB007055.
- DeGrandpre, M.D., Körtzinger, A., Send, U., et al. (2006). Uptake and sequestration of atmospheric CO<sub>2</sub> in the Labrador Sea deep convection region. *Geophysical Research Letters*, 33(21).
- Doney, S.C., Busch, D.S., Cooley, S.R., et al. (2020). The impacts of ocean acidification on marine ecosystems and reliant human communities. *Annual Review of Environment and Resources*, 45(1).
- Doney S.C., Lindsay K., Caldeira K., et al. (2004). Evaluating global ocean carbon models: The importance of realistic physics. *Global Biogeochemical Cycles* 18(3).

- Estournel, C., Testor, P., Damien, P., d'Ortenzio, F., Marsaleix, P., Conan, P., ... & Prieur, L. (2016). High resolution modeling of dense water formation in the north-western Mediterranean during winter 2012–2013: Processes and budget. *Journal of Geophysical Research: Oceans*, 121(7), 5367-5392.
- Fourrier, M., Coppola, L., Claustre, H., et al. (2020). A regional neural network approach to estimate water-column nutrient concentrations and carbonate system variables in the Mediterranean Sea: CANYON-MED. *Frontiers in Marine Science*, 7, 620.
- Fourrier, M., Coppola, L., D'ortenzio, F., et al. (2022). Impact of intermittent Convection in the northwestern Mediterranean Sea on Oxygen content, Nutrients and the Carbonate system. *Journal of Geophysical Research: Oceans*, 127(9).
- Friedlingstein, P., Jones, M.W., O'Sullivan, M., et al. (2022). Global carbon budget 2021. *Earth System Science Data*, 14(4), 1917-2005.
- Friedlingstein, P., O'sullivan, M., Jones, M.W., et al. (2020). Global carbon budget 2020. *Earth System Science Data*, 12(4), 3269-3340.
- Fröb, F., Olsen, A., Pérez, F.F., et al. (2018). Inorganic carbon and water masses in the Irminger Sea since 1991. *Biogeosciences*, 15(1), 51-72.
- Fröb, F., Olsen, A., Våge, K., et al. (2016). Irminger Sea deep convection injects oxygen and anthropogenic carbon to the ocean interior. *Nature communications*, 7(1), 1-8.
- Goris, N., Johannsen, K., & Tjiputra, J. (2022). Gulf Stream and interior western boundary volume transport as key regions to constrain the future North Atlantic Carbon Uptake. *Geoscientific Model Development Discussions*, 1-30.
- Gruber, N., Clement, D., Carter, B.R., et al. (2019). The oceanic sink for anthropogenic CO<sub>2</sub> from 1994 to 2007. *Science*, 363(6432), 1193-1199.
- Heimbürger, L. E., Lavigne, H., Migon, C., d'Ortenzio, F., Estournel, C., Coppola, L., & Miquel, J. C. (2013). Temporal variability of vertical export flux at the DYFAMED time-series station (Northwestern Mediterranean Sea). *Progress in Oceanography*, 119, 59-67.
- Herrmann, M., Diaz, F., Estournel, C., Marsaleix, P., & Ulses, C. (2013). Impact of atmospheric and oceanic interannual variability on the Northwestern Mediterranean Sea pelagic planktonic ecosystem and associated carbon cycle. *Journal of Geophysical Research: Oceans*, 118(10), 5792-5813.
- Holliday, N.P., Waniek, J.J., Davidson, R., et al. (2006). Large-scale physical controls on phytoplankton growth in the Irminger Sea Part I: Hydrographic zones, mixing and stratification. *Journal of Marine Systems*, 59(3-4), 201-218.
- Houpert, L. et al. (2016). Observations of open-ocean deep convection in the northwestern mediterranean sea: Seasonal and interannual variability of mixing and deep water masses for the 2007–2013 period. *J. Geophys. Res. Oceans* 121, 8139–8171. <https://doi.org/10.1002/2016JC011857>
- Jackson, L.C., & Petit, T. (2022). North Atlantic overturning and water mass transformation in CMIP6 models. *Climate Dynamics*, 1-21.

- Karstensen, J., W. Rickels, P. Testor, and M. Telszewski. (2021). Valuing the ocean carbon sink in light of national climate action plans. Pp. 50–51 in *Frontiers in Ocean Observing: Documenting Ecosystems, Understanding Environmental Changes, Forecasting Hazards*. E.S. Kappel, S.K. Juniper, S. Seeyave, E. Smith, and M. Visbeck, eds, A Supplement to *Oceanography* 34(4), <https://doi.org/10.5670/oceanog.2021.supplement.02-21>.
- Kessouri, F., Ulses, C., Estournel, C., Marsaleix, P., Severin, T., Pujo-Pay, M., et al. (2017). Nitrogen and phosphorus budgets in the Northwestern Mediterranean deep convection region. *Journal of Geophysical Research: Oceans*, 122, 9429–9454. <https://doi.org/10.1002/2016JC012665>.
- Kessouri, F., Ulses, C., Estournel, C., Marsaleix, P., D’Ortenzio, F., Severin, T., et al. (2018). Vertical mixing effects on phytoplankton dynamics and organic carbon export in the western Mediterranean Sea. *Journal of Geophysical Research: Oceans*, 123, 1647–1669. <https://doi.org/10.1002/2016JC012669>.
- Khatiwala, S., Tanhua, T., Mikaloff Fletcher, S., et al. (2013). Global ocean storage of anthropogenic carbon. *Biogeosciences*, 10(4), 2169-2191.
- Koelling, J., Atamanchuk, D., Karstensen, J., et al. (2022). Oxygen export to the deep ocean following Labrador Sea Water formation. *Biogeosciences*, 19(2), 437-454.
- Körtzinger, A., Send, U., Lampitt, R.S., et al. (2008). The seasonal pCO<sub>2</sub> cycle at 49°N/16.5°W in the northeastern Atlantic Ocean and what it tells us about biological productivity. *Journal of Geophysical Research: Oceans*, 113(C4).
- Landschützer, P., Laruelle, G. G., Roobaert, A., and Regnier, P. (2020). A uniform pCO<sub>2</sub> climatology combining open and coastal oceans, *Earth Syst. Sci. Data*, 12, 2537–2553, <https://doi.org/10.5194/essd-12-2537-2020>.
- Lauvset, S.K., Key, R.M., Olsen, A., et al. (2016). A new global interior ocean mapped climatology: The 1×1 GLODAP version 2. *Earth System Science Data*, 8(2), 325-340.
- Lauvset, S.K., Lange, N., Tanhua, T., et al. (2021). An updated version of the global interior ocean biogeochemical data product, GLODAPv2. 2021. *Earth System Science Data*, 13(12), 5565-5589.
- Lavigne, H., d’Ortenzio, F., Migon, C., Claustre, H., Testor, P., d’Alcalá, M. R., et al. (2013). Enhancing the comprehension of mixed layer depth control on the Mediterranean phytoplankton phenology. *Journal of Geophysical Research: Oceans*, 118(7), 3416-3430.
- Lee, K., Sabine, C.L., Tanhua, T., et al. (2011). Roles of marginal seas in absorbing and storing fossil fuel CO<sub>2</sub>. *Energy & Environmental Science*, 4(4), 1133-1146.
- Leseurre, C., Lo Monaco, C., Reverdin, G., et al. (2020). Ocean carbonate system variability in the North Atlantic Subpolar surface water (1993–2017). *Biogeosciences*, 17(9), 2553-2577.
- Margirier, F., Testor, P., Heslop, E., Mallil, K., Bosse, A., Houpert, L., ... & Taillandier, V. (2020). Abrupt warming and salinification of intermediate waters interplays with decline of deep convection in the Northwestern Mediterranean Sea. *Scientific Reports*, 10(1), 1-11.
- Marsaleix, P., Auclair, F., Floor, J.W., et al. (2008). Energy conservation issues in sigma-coordinate free-surface ocean models. *Ocean Modelling*, 20(1), 61-89.

- Mertens, C., and F. Schott (1998). Interannual variability of Deep-Water formation in the Northwestern Mediterranean. *J. Phys. Oceanogr.*, 28, 1410–1424
- Metropolis, N., & Ulam, S. (1949). The monte carlo method. *Journal of the American statistical association*, 44(247), 335-341.
- Olivier, L., Boutin, J., Reverdin, G., Lefèvre, N., Landschützer, P., Speich, S., Karstensen, J., Labaste, M., Noisel, C., Ritschel, M., Steinhoff, T., and Wanninkhof, R. (2022). Wintertime process study of the North Brazil Current rings reveals the region as a larger sink for CO<sub>2</sub> than expected, *Biogeosciences*, 19, 2969–2988, <https://doi.org/10.5194/bg-19-2969-2022>.
- Olsen, A., Lange, N., Key, R. et al. (2019). GLODAPv2. 2019—an update of GLODAPv2. *Earth System Science Data*, 11(3), 1437-1461.
- Palevsky, H.I., & Nicholson, D.P. (2018). The North Atlantic biological pump: Insights from the ocean observatories initiative Irminger Sea Array. *Oceanography*, 31(1), 42-49.
- Pérez, F.F., Vázquez-Rodríguez, M., Louarn, E., et al. (2008). Temporal variability of the anthropogenic CO<sub>2</sub> storage in the Irminger Sea. *Biogeosciences*, 5(6), 1669-1679.
- Pérez, F.F., Mercier, H., Vázquez-Rodríguez, M., et al. (2013). Atlantic Ocean CO<sub>2</sub> uptake reduced by weakening of the meridional overturning circulation. *Nature Geoscience*, 6(2), 146-152.
- Pérez, F.F., Fontela, M., García-Ibáñez, M.I., et al. (2018). Meridional overturning circulation conveys fast acidification to the deep Atlantic Ocean. *Nature*, 554(7693), 515-518.
- Pérez, F.F., Treguer, P., Branellec, P., et al. (2020). The 2014 Greenland–Portugal GEOVIDE bottle data (GO–SHIP A25 and GEOTRACES GA01). SEA- NOE.
- Racapé, V., Zunino, P., Mercier, H., et al. (2018). Transport and storage of anthropogenic C in the North Atlantic Subpolar Ocean. *Biogeosciences*, 15(14), 4661-4682.
- Raimondi, L., Tanhua, T., Azetsu-Scott, K., et al. (2021). A 30-Year Time Series of Transient Tracer-Based Estimates of Anthropogenic Carbon in the Central Labrador Sea. *Journal of Geophysical Research: Oceans*, 126(5), e2020JC017092.
- Revelle, R., & Suess, H.E. (1957). Carbon dioxide exchange between atmosphere and ocean and the question of an increase of atmospheric CO<sub>2</sub> during the past decades. *Tellus*, 9(1), 18-27.
- Roemmich D., Wilson W.S., Gould W.J., et al. (2022). The Argo Program. In: *Partnerships in Marine Research*. Elsevier, p 53–69
- Sabine, C.L., Feely, R.A., Gruber, N., et al. (2004). The oceanic sink for anthropogenic CO<sub>2</sub>. *Science*, 305(5682), 367-371.
- Sanleón-Bartolomé, H., Alvarez, M., Velo, A., Tanhua, T., and Fajar, N. M. (2017). The CARIMED (CARbon In the MEDiterranean Sea) Data Synthesis Initiative: Overview And Quality Control Procedures. Available online at: <http://www.repositorio.ieo.es/e-ieo/handle/10508/11313> (accessed October 31, 2019).
- Schneider, A., Tanhua, T., Körtzinger, A., et al. (2010). High anthropogenic carbon content in the eastern Mediterranean. *Journal of Geophysical Research: Oceans*, 115(C12).

Somot, S. et al. (2016). Characterizing, modelling and understanding the climate variability of the deep water formation in the northwestern mediterranean sea. *Clim. Dyn.*. <https://doi.org/10.1007/s00382-016-3295-0>.

Soetaert, K., Hofmann, A.F., Middelburg, J.J., et al. (2007). Reprint of “The effect of biogeochemical processes on pH”. *Marine Chemistry*, 106(1-2), 380-401.

Steinfeldt, R., Rhein, M., Bullister, J.L., et al. (2009). Inventory changes in anthropogenic carbon from 1997–2003 in the Atlantic Ocean between 20S and 65N. *Global Biogeochemical Cycles*, 23(3).

Steinhoff T, Gkritzalis T, Lauvset SK, Jones S, Schuster U, Olsen A, Becker M, Bozzano R, Brunetti F, Cantoni C, Cardin V, Diverrès D, Fiedler B, Fransson A, Giani M, Hartman S, Hoppema M, Jeansson E, Johannessen T, Kitidis V, Körtzinger A, Landa C, Lefèvre N, Luchetta A, Naudts L, Nightingale PD, Omar AM, Pensieri S, Pfeil B, Castaño-Primo R, Rehder G, Rutgersson A, Sanders R, Schewe I, Siena G, Skjelvan I, Soltwedel T, van Heuven S and Watson A (2019). Constraining the Oceanic Uptake and Fluxes of Greenhouse Gases by Building an Ocean Network of Certified Stations: The Ocean Component of the Integrated Carbon Observation System, ICOS-Oceans. *Front. Mar. Sci.* 6:544. doi: 10.3389/fmars.2019.00544

Takahashi, T., Sutherland, S.C., Sweeney, C., et al. (2002). Global sea–air CO<sub>2</sub> flux based on climatological surface ocean pCO<sub>2</sub>, and seasonal biological and temperature effects. *Deep Sea Research Part II: Topical Studies in Oceanography*, 49(9-10), 1601-1622.

Talley, L.D., & McCartney, M.S. (1982). Distribution and circulation of Labrador Sea water. *Journal of Physical Oceanography*, 12(11), 1189-1205.

Touratier, F., L. Azouzi & C. Goyet (2007). CFC-11,  $\Delta^{14}\text{C}$  and 3H tracers as a means to assess anthropogenic CO<sub>2</sub> concentrations in the ocean, *Tellus B: Chemical and Physical Meteorology*, 59:2, 318-325

Touratier F. and C. Goyet (2009). Decadal evolution of anthropogenic CO<sub>2</sub> in the NorthWestern Mediterranean Sea from the mid-1990s to the mid-2000s, *Deep-Sea Res. I*, 56 (2009), pp. 1708-1716

Touratier and Goyet (2011). Impact of the Eastern Mediterranean Transient on the distribution of anthropogenic CO<sub>2</sub> and first estimate of acidification for the Mediterranean Sea, *Deep Sea Research Part I: Oceanographic Research Papers*, Volume 58, Issue 1, January 2011, Pages 1-15 dsr.2010.10.002

Touratier, F., Goyet, C., Houpert, L., de Madron, X. D., Lefèvre, D., Stabholz, M., & Guglielmi, V. (2016). Role of deep convection on anthropogenic CO<sub>2</sub> sequestration in the Gulf of Lions (northwestern Mediterranean Sea). *Deep-Sea Research Part I: Oceanographic Research Papers*, 113, 33–48.

Turner, J.T. (2015). Zooplankton fecal pellets, marine snow, phytodetritus and the ocean’s biological pump. *Progress in Oceanography*, 130, 205-248.

Ulses, C., Auger, P. A., Soetaert, K., Marsaleix, P., Diaz, F., Coppola, L., et al. (2016). Budget of organic carbon in the North-Western Mediterranean open sea over the period 2004–2008 using 3-D coupled physical-biogeochemical modeling. *Journal of Geophysical Research: Oceans*, 121(9), 7026-7055.

Ulses, C., Estournel, C., Marsaleix, P., Soetaert, K., Fourier, M., Coppola, L., Lefèvre, D., Touratier, F., Goyet, C., Guglielmi, V., Kessouri, F., Testor, P., and Durrieu de Madron, X. (in review). Seasonal dynamics and annual budget of dissolved inorganic carbon in the northwestern Mediterranean deep convection region, *Biogeosciences Discuss.* [preprint], <https://doi.org/10.5194/bg-2022-219>, in review, 2022.

Vachon, D. et al. (2020). Paired O<sub>2</sub>–CO<sub>2</sub> measurements provide emergent insights into aquatic ecosystem function. *Limnol. Oceanogr. Lett.* 5, 287–294.

Williams, R.G., & Follows, M.J. (2011). *Ocean dynamics and the carbon cycle: Principles and mechanisms*. Cambridge University Press.

Wolf, M.K., Hamme, R.C., Gilbert, D., et al. (2018). Oxygen saturation surrounding deep water formation events in the Labrador Sea from Argo-O<sub>2</sub> data. *Global Biogeochemical Cycles*, 32(4), 635-653.

Zunino, P., García-Ibáñez, M.I., Lherminier, P., et al. (2014). Variability of the transport of anthropogenic CO<sub>2</sub> at the Greenland–Portugal OVIDE section: controlling mechanisms. *Biogeosciences*, 11(8), 2375-2389.

Zunino, P., Mercier, H., & Thierry, V. (2020). Why did deep convection persist over four consecutive winters (2015–2018) southeast of Cape Farewell? *Ocean Science*, 16(1), 99-113.